The Concept of "Normalized" Distribution to Describe Raindrop Spectra: A Tool for Cloud Physics and Cloud Remote Sensing

JACQUES TESTUD AND STÉPHANE OURY

Centre d'Etudes des Environnements Terrestres et Planétaires, Institut Pierre-Simon Laplace, Velizy, France

ROBERT A. BLACK

Hurricane Research Division, NOAA/Atlantic Oceanographic and Meteorological Laboratory, Miami, Florida

PAUL AMAYENC

Centre d'Etudes des Environnements Terrestres et Planétaires, Institut Pierre-Simon Laplace, Velizy, France

XIANKANG DOU

Department of Earth and Space Sciences, University of Science and Technology of China, Hefei, Anhui, China

(Manuscript received 23 February 2000, in final form 10 August 2000)

ABSTRACT

The shape of the drop size distribution (DSD) reflects the physics of rain. The DSD is the result of the microphysical processes that transform the condensed water into rain. The question of the DSD is also central in radar meteorology, because it rules the relationships between the radar reflectivity and the rainfall rate R. Normalizing raindrop spectra is the only way to identify the shape of the distribution. The concept of normalization of DSD developed in this paper is founded upon two reference variables, the liquid water content LWC and the mean volume diameter D_m. It is shown mathematically that it is appropriate to normalize by $N_0^* \propto \mathrm{LWC}/D_m^4$ with respect to particle concentration and by D_m with respect to drop diameter. Also, N_0^* may be defined as the intercept parameter that would have an exponential DSD with the same LWC and D_m as the real one. The major point of the authors' approach is that it is totally free of *any assumption* about the shape of the DSD. This new normalization has been applied to the airborne microphysical data of the Tropical Ocean and Global Atmosphere Coupled Ocean–Atmosphere Response Experiment (TOGA COARE) collected by the National Center for Atmospheric Research Electra aircraft. The classification of the TOGA COARE raindrop spectra into four categories [one stratiform, and three convective (0–10, 10–30, and 30–100 mm h^{-1})] allowed the following features to be identified.

1) There is a distinct behavior of N_0^* between stratiform and convective rains; typical values are $2.2 \times 10^6\ \mathrm{m}^{-4}$ for stratiform and $2 \times 10^7\ \mathrm{m}^{-4}$ for convective.
2) In convective rain, there is a clear trend for D_m to increase with R, but there is *no correlation* between N_0^* and R.
3) The "average" normalized shape of the DSD is remarkably stable among the four rain categories. This normalized shape departs from the exponential, but also from all the analytical shapes considered up to now (e.g., gamma, lognormal, modified gamma).

The stability of the normalized DSD shape and the physical variability of N_0^* and D_m are discussed in respect to the equilibrium theory of List et al. The stability of the shape implies that two parameters (and only two) are needed to describe the DSD. This stability supports the robustness of rain relations parameterized by N_0^*. The same TOGA COARE dataset is used to check that the rain relations parameterized by N_0^* are much less dispersed than the classical ones, even after rain-type classification.

1. Introduction

From the early work by Marshall and Palmer (1948), a considerable number of papers have been published on the subject of the raindrop size distribution (DSD). The motivation for such an interest is threefold:

1) the shape of the distribution reflects the physics of rain, that is, the more or less complex microphysical processes (warm and cold) that transform the condensed water into rain;
2) the quantitative estimate of rain from microwave remote sensing, active (weather radar) or passive (microwave radiometer), is subject to the natural variability of the DSD characteristics; and
3) to design radio links for telecommunications and to

Corresponding author address: Jacques Testud, CETP-UVSQ, 10-12 avenue de l'Europe, 78140 Vélizy, France.
E-mail: testud@cetp.ipsl.fr

evaluate the fading caused by rain, it is important to have good DSD models.

Early ground-based DSD measurements used filter paper (Marshall and Palmer 1948) or the so-called flour method (Law and Parsons 1943). The most widespread technique today is the disdrometer (Joss and Walvogel 1967). However, it is worth mentioning optical techniques like the optical spectropluviometer (Hauser et al. 1984) or the recent 2D video disdrometer (Schönhuber et al. 1996; Urban et al. 1996). At altitude, DSD observations are also currently obtained from particle measuring systems (PMS) optical array probes on aircraft (Knollenberg 1970, 1981).

A common difficulty with all of these sensors is related to the small collection area of the instrument, which makes the drop counting in each diameter class very noisy, especially for large drops, which have the smallest concentration. Thus, it is not easy to find a satisfactory compromise for the integration time: if long, it may smooth actual physical variations; if short, the observed DSD may be dominated by counting fluctuations.

The most widely used mathematical shape to represent DSDs is the exponential distribution $N(D) = N_0 \exp(-\Lambda D)$, where N is concentration of raindrops per diameter interval D, N_0 is the intercept parameter, and Λ is the slope parameter [as in Marshall and Palmer (1948)] or the gamma distribution $N(D) = N_0 D^{\mu} \exp(-\Lambda D)$ (as in Willis 1984). Occasionally, the modified gamma (Best 1950; Law and Parsons 1943) or lognormal (Markowitz 1976; Feingold and Levin 1986) distributions have been used. Marshall and Palmer have shown that, at weak or moderate rainfall rate, average distributions, after being sorted by class of rainfall rate, are reasonably close to exponential and intercept the axis of zero diameter at a ''fixed'' N_0 value ($\cong 0.8 \times 10^7$ m^{-4}). They deduced a very simple parameterization of the DSD as a function of rainfall rate that is still widely used. Joss and Gori (1978) noted that if after accumulation during long intervals the DSD is generally found to be close to the exponential, the ''instant'' DSD (integrated over 1 min) departs markedly from the exponential. The gamma distribution has been introduced to account better for the shape of the distribution at high rainfall rate observed by disdrometers, characterized by a deficit of small drops and by a convexity of the ''tail'' of the DSD for large drop diameters. Nevertheless, the counting of small drops by the Joss and Waldvogel impact disdrometer is negatively biased. This effect, which takes more and more importance as the rainfall rate increases, was already discussed by Joss and Gori (1976) and has been recently documented by simultaneous observations with a video disdrometer (Williams et al. 2000). A drawback of the gamma distribution is that the intercept parameter N_0 can no longer be considered to be a physical quantity, because its *dimension itself* is ill defined. To overcome this difficulty, Chandrasekar and Bringi (1987) proposed to use the total number of particles n_T instead of N_0 in the gamma DSD formulation. Nevertheless, this remedy is only partial; the normalized gamma DSD (Willis 1984; Dou et al. 1999; Testud et al. 2000) is a much more satisfactory formulation.

The question of the DSD is central in radar meteorology, that is, in the problem of the relationships between radar observables (such as equivalent radar reflectivity Z) and physical parameters (such as rainfall rate R or precipitation liquid water content LWC). Driven by the problem of interpreting classical weather radar data, the parameterization of the DSD by a single parameter (generally R) has been proposed by several authors. Since the earlier parameterization by Marshall and Palmer, the most synthetic work is probably that by Ulbrich (1983), who presented a systematic approach to calculate the relationships between any couple of integral parameters of the distribution, assuming a gamma shape for the DSD. In the framework of the current paper, it is also relevant to cite Sempere Torres et al. (1998) who described a general approach to parameterize the DSD from a single parameter (e.g., R). Marshall and Palmer's parameterization implies that all the moments of the distribution are related through power-law relationships, but Sempere Torres et al. postulated the existence of such power laws to establish a normalization of the DSD as $N(D, R) = R^{\alpha} g(R^{-\beta} D)$, where R^{α} and R^{β} are the normalization factors in concentration and diameter, respectively, and $g(X)$ is the ''intrinsic shape'' of the normalized DSD.

The collisional interaction of raindrops and their resulting coalescence and breakup has been recognized for a long time to be the major process that determines the shape of the DSD (Srivastava 1971). Low and List's (1982a,b) parametric description of the coalescence–breakup process is the most widely used reference in studies of the evolution of the DSD. The ''equilibrium distribution'' resulting from the equilibrium between coalescence and breakup (in absence of source or sink terms like condensation, evaporation, and advection), has been the object of a number of numerical studies (Valdez and Young 1985; Brown 1986, List et al. 1987; Hu and Srivastava 1995). All of them agree in the conclusion that all equilibrium distributions are proportional. Zawadzki and Agostinho Antonio (1988) showed the existence of ''natural'' DSDs (corresponding to heavy tropical rain) compatible with the concept of an equilibrium distribution. However, as pointed out by List et al. (1987), the equilibrium distribution implies that all moments are proportional and, in particular, that the Z–R relationship is *linear*, in contradiction to observation (Battan 1973).

The object of the current paper is threefold:

1) to propose an approach for the normalization of the DSD independent from any assumption about its mathematical shape or from any postulate about the relationship between its moments,

2) to propose a new parameterization of the relationships between integral parameters of the DSD, and
3) to apply these concepts extensively to an airborne microphysical dataset and to discuss the results in respect to the concept of equilibrium DSD.

2. A general concept for normalizing DSDs

This section first describes the mathematical basis of the normalization of raindrop spectra. Illustration of application is then given, first considering classical functional forms (exponential, gamma DSDs) and second the List et al. (1987) form of the equilibrium DSD.

a. Mathematical formulation

The physical characterization of any observed raindrop spectrum raises three questions:

1) What ''rain intensity'' corresponds to this spectrum?
2) What is the ''mean'' drop diameter?
3) What is the ''intrinsic'' shape of the dropsize distribution?

To characterize ''rain intensity,'' two parameters may be considered: the liquid water content (g m^{-3}), or the rainfall rate (mm h^{-1}). Traditionally, R is more often adopted than LWC. However it may be argued that LWC is a better parameter than R, because it has a clearer physical meaning (at altitude, R is subject to vertical air motion and change in terminal fall velocity related to air density). There is no ambiguity in the definition of LWC. It is simply proportional to the third moment of the drop size distribution $N(D)$, where N is number of particles per unit volume and per interval of diameter (m^{-4}) and D is drop diameter (m). More specific,

$$\mathrm{LWC} = \frac{\pi\rho_w}{6}\int_0^\infty N(D)D^3\,dD. \tag{1}$$

The definition of the ''mean'' diameter is a little more arbitrary. What is used traditionally in radar meteorology is the ''median volume diameter'' D_0, defined as the drop diameter sharing in two equal parts the liquid water content. Less often people use the ''volume-weighted'' mean diameter D_m (generally referred to as the ''mean volume diameter''), defined as the ratio of the fourth to the third moments of the DSD:

$$D_m = \frac{\displaystyle\int_0^\infty N(D)D^4\,dD}{\displaystyle\int_0^\infty N(D)D^3\,dD}. \tag{2}$$

Here, D_m is, in fact, very close to the median volume diameter D_0. Ulbrich (1983) stated that, for a Gamma distribution, $D_m = (4 + \mu)/(3.67 + \mu)D_0$. He noticed that, provided μ is less than or equal to -1 (which is the case for most of the natural DSDs), D_m is a very good approximation to D_0. Ulbrich even proposed to use D_m as an estimator of D_0 (because D_0 is not easy to calculate directly). In this paper, D_m is chosen to characterize the mean drop diameter of the DSD. It is physically as meaningful as D_0 while being much easier to calculate from observed spectra or to manipulate in theoretical computations.

The definition of the intrinsic shape is intimately related to the concept of normalization of raindrop spectra. Normalization is interesting when it is intended to compare the shape of two spectra that have not the same LWC and/or D_m. Thus, normalization should be defined in such a way that the intrinsic shape is independent of LWC and/or D_m. A general expression of the normalization of the DSD is

$$N(D) = N_0^* F(D/D_m), \tag{3}$$

where N_0^* is the scaling parameter for concentration and D_m is the scaling for diameter. Here, $F(X)$ in (3) denotes the ''normalized DSD'' describing the intrinsic shape of the DSD (noting that $X = D/D_m$). By virtue of (2), $F(X)$ obeys the following integral equation:

$$\int_0^\infty F(X)X^4\,dX = \int_0^\infty F(X)X^3\,dX. \tag{4}$$

Meanwhile (1) provides

$$\int_0^\infty F(X)X^3\,dX = \frac{6}{\pi\rho_w}\frac{\mathrm{LWC}}{N_0^* D_m^4}. \tag{5}$$

For the normalized function F to be independent of LWC and D_m, it should be required that

$$\int_0^\infty F(X)X^3\,dX = C, \tag{6}$$

where C is an arbitrary constant. In this paper, constant C is *arbitrarily* taken to be

$$C = \Gamma(4)/4^4. \tag{7}$$

This choice will be justified in the next section. It follows from (6) and (7) that N_0^* is defined by

$$N_0^* = \frac{4^4}{\pi\rho_w}\frac{\mathrm{LWC}}{D_m^4}. \tag{8}$$

It is interesting to note that the normalization defined by (8) is very similar to that proposed by Sekhon and Srivastava (1971), Willis (1984), and Testud et al. (2000) (except with the choice of D_m instead of D_0). Although, however, the DSD was assumed to be exponential in Sekhon and Srivastava (1971) and gamma in Willis (1984) and Testud et al. (2000), in the current approach *there is absolutely no assumption on the shape of the DSD.*

b. Application of the normalization to an exponential DSD

For an exponential DSD of the form $N(D) = N_0 \exp(-\Lambda D)$, the ith-order moment is expressed as

$$M_i = \int_0^\infty D^i N(D)\, dD = N_0 \frac{\Gamma(i+1)}{\Lambda^{i+1}}. \quad (9)$$

It follows that the mean volume diameter D_m is given by:

$$D_m = M_4/M_3 = 4/\Lambda. \quad (10)$$

Parameter N_0^* may be calculated as

$$N_0^* = \frac{4^4}{\pi\rho_w}\frac{\mathrm{LWC}}{D_m^4} = \frac{4^4}{\Gamma(4)}\frac{M_3^5}{M_4^4} = N_0. \quad (11)$$

Last, the normalized form of the exponential DSD, $F(X)$, is expressed as

$$F(X) = \exp(-4X). \quad (12)$$

Obviously it is not by chance, but due to our specific choice of constant C, that $N_0^* = N_0$ for the exponential DSD. This equality justifies the notation of parameter N_0^* and allows us to give a simple physical interpretation of it: *whatever the shape of an observed DSD is, the corresponding N_0^* is the intercept parameter of the exponential DSD with the same LWC and D_m.*

c. Normalization for a gamma DSD

For a gamma DSD of the form $N(D) = N_0 D^\mu \exp(-\Lambda D)$, the ith-order moment expresses as

$$M_i = N_0 \frac{\Gamma(i+\mu+1)}{\Lambda^{i+\mu+1}}. \quad (13)$$

The corresponding median volume diameter D_m is given by

$$D_m = M_4/M_3 = (4+\mu)/\Lambda, \quad (14)$$

and parameter N_0^* may be calculated as

$$N_0^* = \frac{4^4}{\Gamma(4)}\frac{M_3^5}{M_4^4} = N_0 D_m^\mu \frac{\Gamma(4+\mu)}{\Gamma(4)}\frac{4^4}{(4+\mu)^{4+\mu}}. \quad (15)$$

It follows that the normalized shape of the DSD is

$$F_\mu(X) = \frac{\Gamma(4)}{4^4}\frac{(4+\mu)^{4+\mu}}{\Gamma(4+\mu)} X^\mu \exp[-(4+\mu)X]. \quad (16)$$

Thus it turns out that the normalized expression of the gamma DSD is

$$N(D) = N_0^* F_\mu(D/D_m). \quad (17)$$

Despite the complexity of (17) [through (16)], the major interest of the normalization for a gamma DSD is that now the three parameters N_0^*, D_m, and μ have a clear physical meaning: D_m represents a mean particle size, N_0^* is the intercept parameter of the exponential distribution of same LWC and D_m, and μ is confined to the description of the shape of the DSD. In contrast, with the classical formulation of the gamma DSD, the intercept parameter N_0 and slope parameter Λ represent a mixture of the LWC, D_m, and shape. The intercept parameter N_0 is particularly problematic. As already pointed by Chandrasekar and Bringi (1987), N_0 is affected by strong variation—physically senseless—correlated with that of μ (for fixed N_0^* and D_m, when μ varies from -2 to $+4$, N_0 varies over three decades). Further, N_0's *dimension itself* ($\mathrm{m}^{-4-\mu}$) is ill defined.

To overcome this problem, Chandrasekar and Bringi (1987) suggest using the total number of particles n_T in the formulation of the gamma DSD. However, this solution is only partial: if n_T is well dimensioned (m^{-3}), it nevertheless exhibits correlated variations with μ that are small for μ greater than 0 (relative variation by a factor of 5 for μ varying from 0 to 4) but are amplified when approaching μ equal to -1 (for which n_T tends to infinity).

d. Normalization of List et al.'s (1987) equilibrium DSD

From List et al. (1987), the equilibrium DSDs consist of a family of curves "that are multiples of one another," parameterized by the rainfall rate as

$$N(D) = f(D,R) = R\psi(D), \quad (18)$$

where $\psi(D)$ is a shape function.

It appears immediately that all the curves of the family have a common mean volume diameter given by

$$D_m = \frac{\int_0^\infty \psi(D) D^4\, dD}{\int_0^\infty \psi(D) D^3\, dD}. \quad (19)$$

Then N_0^* is given by

$$N_0^* = \frac{4^4}{\Gamma(4)}\frac{\left[\int_0^\infty \psi(D) D^3\, dD\right]^5}{\left[\int_0^\infty \psi(D) D^4\, dD\right]^4} R. \quad (20)$$

The invariant character in the drop spectrum shape $\psi(D)$ (predicted by the coalescence–breakup numericals models) implies that, for equilibrium DSDs,

1) D_m is a constant (prescribed by the theory),
2) N_0^* is proportional to R, and
3) $F(X)$ $[=R/N_0^*\psi(XD_m)]$ is prescribed by the theory.

Thus the present normalization is a good approach to test the equilibrium theory from experimental raindrop spectra.

3. Relationships between moments of the DSD

Moments of the DSD represent more or less faithfully most of the integral parameters of the DSD of interest for a radar meteorologist. For example, LWC is proportional to M_3; R is proportional to $M_{3.67}$ (assuming that the terminal fall velocity is $V_t \propto D^{0.67}$), Z is proportional to M_6, and the specific attenuation K is pro-

TABLE 1. Variation of the a coefficient of the relationship $Z/N_0^* = a(R/N_0^*)^{1.5}$ with the shape parameter μ of the normalized gamma DSD.

μ	-0.5	0	1	2	3	4	5
a	7.02×10^5	6.48×10^5	5.76×10^5	5.30×10^5	4.99×10^5	4.76×10^5	4.59×10^5

portional to M_3 (the last one, under the Rayleigh approximation). Ulbrich (1983) presented a systematic approach to calculate the relationships between integral parameters of the DSD, assumed to be a gamma distribution. It is not the ambition here to reproduce his thorough study of the question, but only to show that our normalization allows generalization of his approach to any DSD shape. A general expression of the ith-order moment of the DSD is

$$M_i = \int N_0^* F(D/D_m) D^i \, dD = N_0^* D_m^{i+1} \xi_i, \quad (21)$$

where ξ_i is the ith-order moment of the *normalized distribution* $F(X)$,

$$\xi_i = \int F(X) X^i \, dX. \quad (22)$$

Thus, between two moments of order i and j, the following relationship stands:

$$\frac{M_i}{N_0^*} = \xi_i \xi_j^{-[(i+1)/(j+1)]} \left(\frac{M_j}{N_0^*} \right)^{[(i+1)/(j+1)]}, \quad (23)$$

with N_0^* ranging typically between 10^6 and 10^8 m^{-4}.

Equation (23) establishes that, *when normalized by* N_0^*, the relationship between two moments of order i and j of the DSD is a power law whose exponent is $(i + 1)/(j + 1)$, *independent of the shape of the DSD*. This is a remarkable result of the normalization. With classical gamma DSDs, Ulbrich (1983) established similar power-law relationships but with exponent $(i + \mu + 1)/(j + \mu + 1)$, thus showing shape dependence. Using a *normalized* gamma (or any other mathematical shape, provided it is normalized), this dependence disappears.

Taking the particular instance of the Z–R relationship as $Z = M_6$ and $R \propto M_{3.67}$ (with a power law as $V_t \propto D^{0.67}$ for terminal fall velocity), (23) sets the exponent of the Z/N_0^*–R/N_0^* relationship to $7/4.67 \cong 1.5$. Thus it may be written that

$$Z/N_0^* = a(R/N_0^*)^{(1.5)} \quad \text{or} \quad Z = aN_0^{*(-0.5)} R^{1.5}. \quad (24)$$

For R (mm h^{-1}), Z (mm^6 m^{-3}), N_0^* (m^{-4}), and with the terminal fall velocity law $V_t = 386.6D^{0.67}$ (V_t: m s^{-1}, D: m) (Atlas and Ulbrich 1977), it is found that

$$a = 5.2 \times 10^4 \xi_6 \xi_{3.67}^{-1.5}. \quad (25)$$

By virtue of the normalization, a depends only on the shape of the DSD. Moreover, this dependence is necessarily moderate, because the third and the fourth normalized moments ξ_3 and ξ_4 are by definition equal to $\Gamma(4)/4^4$, which strongly constrains the neighboring moments (such as $\xi_{3.67}$ or, to lesser extent, ξ_6). For a normalized Gamma DSD, Table 1 displays the variation of the a coefficient [defined by (25)] as a function of the shape parameter μ. It can be seen that the relative variation of a over the full interval $-0.5 < \mu < 5$ is about $\pm 20\%$ around a mean of 5.8×10^5, which imparts a variation of ± 0.8 dBZ in the definition of Z derived from (24) at given R. Meanwhile the natural variability of N_0^* is ± 10 dB, which imparts a variability of ± 5 dBZ in the radar reflectivity derived from (24). Thus N_0^* is probably a key parameter to monitor the variability of the Z–R relationship due to the DSD, the effect of the shape being of secondary importance.

One should not be mistaken about the practical significance of (24). This equation *does not mean* that the exponent of the Z–R relationship should be 1.5. It does not even imply that any functional relationship exists between Z and R. Indeed if there is no correlation between the two parameters LWC and D_m characterizing any DSD, it is expected that the correlation between N_0^* ($\propto$LWC/D_m^4) and LWC will be weak, as is the correlation between N_0^* and R (given that R is highly correlated to LWC). In such circumstances, (24) implies a Z–R relationship *randomized by* N_0^*, not a functional relationship. When it is assumed that N_0^* is constant (which implies a functional relationship as LWC $\propto D_m^4$), (24) becomes coincident with the Marshall–Palmer parameterization, expressing a power-law Z–R relationship with exponent 1.5. Note nevertheless that the present result is obtained *without any assumption on the shape* of the DSD. If we set N_0^* to 0.8×10^7 m^{-4} [the value adopted by Marshall and Palmer (1948) for the intercept parameter N_0 of their exponential DSD] and the shape parameter μ to 1, it is found that $Z = 204R^{1.5}$ (R: mm h^{-1}, Z: mm^6 m^{-3}). But (24) is *also compatible* with the linear Z–R relationship implied by List et al.'s (1987) equilibrium theory. As shown in section 2d, within the framework of this theory, N_0^* is proportional to R; thus (24) implies a *linear* Z–R relationship as in List (1988).

The normalization technique developed in this paper should not be considered as a theory, but only as a *mathematical technique* that helps in analyzing properties of raindrop spectra and in evaluating their consequence on the relationships between integral parameters of the DSDs. Its strength is that it does not constrain the data analysis by any a priori assumption, either on the shape of the DSD or on the relationships between moments of the DSD. It lets experimental facts decide what this shape is and what these relationships are. In particular, it is perfectly neutral with respect to the Z–R relationship. It is absolutely candid about questions

TABLE 2. Coefficient γ_P in (27) and relative error in the parameters determined by the method of moments for $u_s = 1.15$ m^3, $N_0^* = 10^7$ m^{-4}, and $D_m = 1.3$ mm.

Parameter	LWC	R	Z	D_m	N_0^*
γ_P	4.47	6.79	30.39	4.47	14.83
$\sigma(P)/P$ (% and dB)	7.31%	11.10%	49.71% (1.75 dBZ)	7.31%	24.25%

such as: ''Is the Z–R relationship linear or a power law?'' or even: ''Does any functional relationship exist between Z and R?''

4. Application of the normalization to TOGA COARE airborne microphysical data

a. Airborne microphysical data in TOGA COARE

The Tropical Ocean and Global Atmosphere Coupled Ocean–Atmosphere Response Experiment (TOGA COARE) took place in the west Pacific Ocean from November of 1992 to February of 1993. This experiment, whose description can be found in Webster and Lucas (1992), deployed a number of oceanographic ships and instrumented aircraft. The National Center for Atmospheric Research (NCAR) Electra aircraft accomplished 21 flights out of Honiara, Guadalcanal, to observe deep convection over the warm pool of the west Pacific Ocean. Among the instrumentation on this aircraft was a two-dimensional precipitation PMS probe (2D-P), whose data were analyzed following the procedure described in Atlas et al. (2000). The PMS data were integrated over 6 s (i.e., about 800 m along track considering an aircraft speed of 135 m s^{-1}) to obtain raindrop spectra with diameters from 0.2 to 6.4 mm at a resolution of 0.2 mm (32 diameter classes). The collection area of the 2D-P probe is about 1600 mm^2 and the sampling volume u_s for each spectrum is $\sim$1.15 m^3. In total, 7112 spectra were collected during the 21 flights in question. During most flights, the Electra was cruising at about 3-km altitude, well below the freezing level (which is between 4.5 and 5 km in this area of the globe).

For each spectrum, the third and fourth moments are calculated, from which LWC, D_m, and N_0^* are subsequently determined. The rainfall rate R is calculated assuming Atlas and Ulbrich's (1977) law for terminal fall velocity,

$$V_t(D) = 386.6D^{0.67}, \tag{26}$$

(V_t: m s^{-1}; D: m). The equivalent radar reflectivity Z_e and K are calculated using a Mie scattering model. An evaluation of the statistical errors in LWC, R, Z_e, D_m, and N_0^* calculated by this procedure is presented in the appendix. In this error evaluation, to make the calculation analytically tractable, R and Z_e are assimilated to moments of the DSD, the drop counting is assumed obeying Poisson statistics, and the DSD is exponential. The appendix establishes [see (A24)] that the relative standard deviation in parameter P (representing any of N_0^*, D_m, LWC, R, or Z_e) is

$$\sigma(P)/P = 2\gamma_P/(u_s N_0^* D_m)^{1/2}, \tag{27}$$

where γ_P is the coefficient attached to parameter P.

Table 2 displays γ_P for the above-mentioned parameters and indicates ''typical'' relative errors obtained with a sampling volume $u_s = 1.15$ m^3 and an exponential DSD characterized by $N_0^* = 10^7$ m^{-4} and $D_m = 1.3$ mm. It can be seen that Z, as a higher moment of the DSD than LWC or R, is affected by more uncertainty. Meanwhile D_m and, to lesser extent, N_0^* are fairly well determined.

Systematic errors are also expected 1) from the truncation of the spectra with drops above 6.5 mm in drop diameter and 2) from the deficit of drop counting with the 2D-P probe at the three smallest classes of diameter (about 40% at 0.2 mm and 10% at 0.4 and 0.6 mm). The second effect is partially compensated for by decreasing the collection area by two pixels (or 6.25%), for drops with diameter smaller than 0.5 mm. These systematic errors may be easily evaluated by assuming an analytical shape of the DSD (exponential, or the so-called modified exponential defined in section 5d). The truncation error is found to be less than 1% for all parameters mentioned in Table 2. The small drop deficit counting, after compensation as mentioned above, is found to induce a bias of about -1% in LWC, $+0.5$% in D_m, and -3% in N_0^*, when D_m is 1 mm. This bias decreases as D_m increases.

b. Rain classification

For the purposes of this study, a classification of the precipitation as ''stratiform'' or ''convective'' is made using a simple criterion expressing the character of stratiform rain to be ''extended horizontally'' and ''weak.'' This criterion is as follows. Consider an along-track series $\{R_i\}$ of the rainfall rate (subscript i stands for each individual spectrum). If R_k and the ten adjacent values (from R_{k-5} to R_{k+5}), are all less than 10 mm h^{-1}, then spectrum k is considered to be stratiform rain; otherwise, spectrum k is classified as convective.

This criterion allows classifying as convective a low rainfall-rate spectrum within the influence radius of a convective rain cell (this influence radius being fixed to $\pm$3.6 km). A result of such a classification along aircraft track is illustrated in Fig. 1, corresponding to the flight of 14 December 1992.

It is interesting to compare the current classification scheme with that considered by Tokay and Short (1996) in their analysis of disdrometer data collected at Kapingamarangi during TOGA COARE. From a case

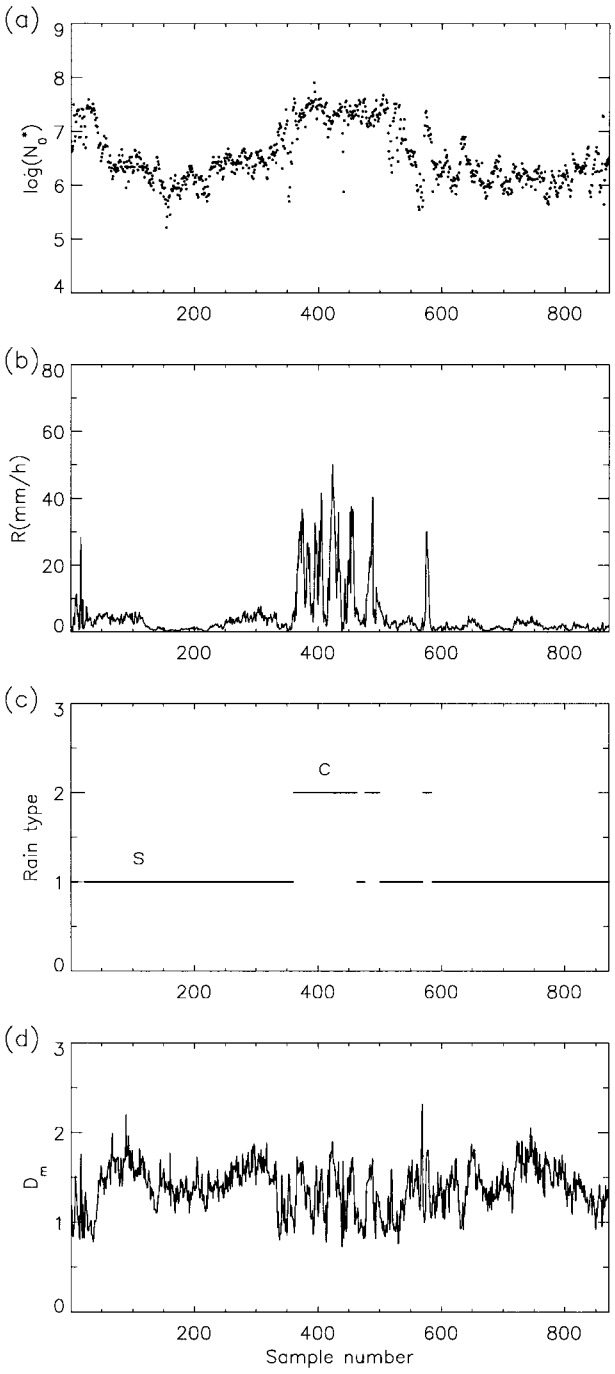

FIG. 1. TOGA COARE flight of the NCAR Electra (14 Dec 1992). Alongtrack variation of (a) $\log(N_0^*)$, (b) rainfall rate R (mm h^{-1}), (c) rain type: stratiform (1) or convective (2), and (d) mean volume diameter D_m. One hundred samples represent 80 km along track.

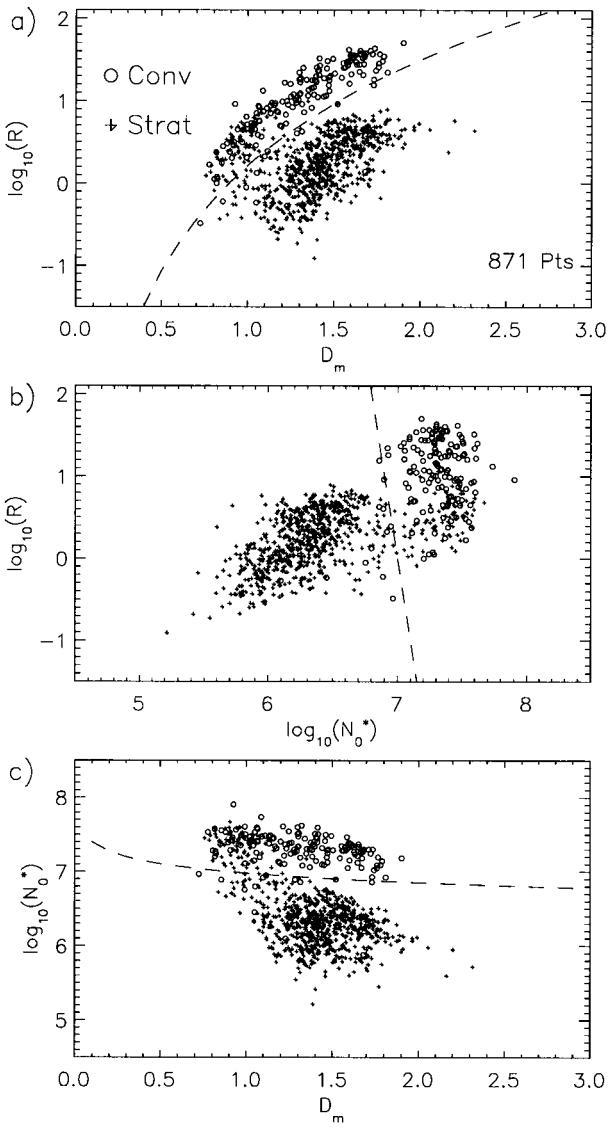

FIG. 2. For the 14 Dec 1992 flight, scatterplot of (a) $\log(R)$ vs D_m, (b) $\log(R)$ vs $\log(N_0^*)$, and (c) $\log(N_0^*)$ vs D_m. Circles and dots correspond to rain spectra classified as convective or stratiform, respectively, by the simple classification scheme. Dashed lines visualize the criterion for Tokay and Short–type classification (see text).

study, Tokay and Short observed that, in a diagram of R versus N_0 (where N_0 is the intercept parameter of the classical gamma DSD), stratiform and convective rain spectra occupy two distinct domains, delimited by a N_0–R relationship as $N_0 = 4 \times 10^9 \mathrm{R}^{-4.3}$. This relation forms the basis of their classification. Tokay and Short's criterion cannot be used directly in this study, because N_0^* is very different from the intercept parameter of a gamma DSD. However, in the same spirit, Fig. 2 displays, for the above-cited 14 December 1992 flight, scatter plots of R versus D_m, R versus N_0^*, and D_m versus N_0^*. In each scatterplot, the datapoints are organized in two distinct clusters, just as Tokay and Short observed it with R, N_0, and Λ. The separation lines are, respectively (R: mm h^{-1}, N_0^*: m^{-4}, and D_m: mm):

$$R = 1.64 D_m^{4.25} \tag{28}$$

$$N_0^* = 10^7 R^{-0.1}, \quad \text{and} \tag{29}$$

$$N_0^* = 0.95 \times 10^7 D_m^{-0.42}. \tag{30}$$

These three relations are built to be consistent with the quasi-functional relationship $R \propto \xi_{3.67} N_0^* D_m^{3.67}$ [with $\xi_{3.67} \approx \Gamma(4)/4^4$], that can be derived from (21). Equation (29) is used in the following, to practice an alternative classification referred to as ''Tokay and Short type'' or ''TS type.'' With respect to the other TS-type classification, the rate of ''misclassification'' of stratiform rain by the ''simple'' scheme (percentage of dots falling above the separation lines) is 7.1%. That for convective rain (percentage of circles falling below the separation lines) is 6.1%. If we extend the statistics to the 7112 rain spectra of the full dataset, the misclassification rate rises to 18% for convective and 12% for stratiform. Note that this rise should not necessarily be interpreted as a worse performance of the simple scheme; it may also reflect a variation of the transition defined by (29) from one meteorological situation to the other.

The ensemble of the TOGA COARE raindrop spectra was finally classified into four categories: stratiform (S); convective ($0 < R \leq 10$ mm h^{-1}) (C/0–10); convective ($10 < R \leq 30$ mm h^{-1}) (C/10–30), and convective ($R > 30$ mm h^{-1}) (C/30–100).

c. Procedure to average normalized spectra

From each component of the observed spectrum $N(D_i)$, the corresponding component of the normalized spectrum $F(X_i)$ is calculated according to (3) as

$$F(X_i) = N(D_i)/N_0^*. \tag{31}$$

Where $X_i = D_i/D_m$. Then one considers classes in ''normalized diameter'' X, with width of 0.1 (the first class is centered over $X = 0.05$ and the last one on $X = 3.95$), and calculates the average $\overline{F}(X)$ and standard deviation $\sigma[F(X)]$ of all $F(X_i)$ falling in each class.

d. Best-fitting normalized gamma distribution

For each individual normalized spectrum $F(X_i)$, one determines the best-fitting ''normalized gamma distribution.'' This is accomplished by determining the μ parameter that realizes the least squares fit of $\log[F_\mu(X)]$, defined in (16), to $\log[F(X_i)]$. This is a *one-parameter* adjustment, as opposed to a procedure with the classical gamma DSD that would consist of a nonlinear adjustment of the three parameters N_0, Λ, and μ and where the estimates of the three parameters interact among each other. In this procedure, N_0^* and D_m are determined *beforehand*, independently of any hypothesis on the shape of the DSD. Then μ is determined without possibility of influencing N_0^* and D_m, which improves the stability of its retrieval. Nevertheless, because the criterion for successful fit is based on a χ^2 test, the convergence of the nonlinear least squares fit routine is sometimes problematic with low rain-rate spectra for which the statistical fluctuation of $F(X_i)$ is large.

5. Statistical properties of the DSDs observed in TOGA COARE

The results of the classification and normalization procedure are summarized in Figs. 3–6. For each precipitation category, Figs. 3–6 display

1) the histograms of R, N_0^*, D_m, and μ parameter;
2) a scatterplot of all normalized spectra of the category;
3) for reference, a scatterplot of the same spectra without normalization; and
4) the average spectrum $\overline{F}(X)$ with its standard deviation.

a. Results for stratiform rain

For the 5381 spectra classified as stratiform rain (Fig. 3), the $\log(N_0^*)$ histogram exhibits a well-defined peak near 6.2 but also a shoulder near 7.2. The overall span of the histogram is from 5.3 to 7.7, with its average at 6.49. The D_m histogram typically extends from 0.6 to 1.8 mm. The μ histogram covers typically the interval $-1 < \mu < +2$.

Despite this large variability in N_0^* and D_m, the dispersion between the various normalized spectra (Fig. 3e) is moderate, especially when compared with that obtained without normalization (Fig. 3f). The average spectra $\overline{F}(X)$ is close to the exponential [$F(X) = \exp(-X)$], but exhibits nevertheless a tendency to a bow shape with a slight convexity beyond $X = 0.5$. The standard deviation {represented by an ''error bar'' [$\overline{F}(X) - \sigma$; $\overline{F}(X) + \sigma$]} is moderate as long as $X < 1.5$ and then amplifies rapidly for $X \geq 1.5$. This sudden amplification is an effect of the log representation: when $\sigma/\overline{F}(X)$ reaches 1, the lower bound of the error bar goes to negative infinity. The error bar representation shows that the tail of the normalized distribution is subject to large fluctuations. Most of these fluctuations are expected to be statistical in nature, as demonstrated hereinafter. Under the hypothesis that the drop counting in each diameter class obeys a Poisson distribution, the appendix [see (A5)] calculates the standard deviation of $F(X_i)$ as

$$\sigma\{F(X_i)\}/\overline{F}(X_i) = [u_s N_0^* \overline{F}(X_i) \Delta D]^{-1}. \tag{32}$$

Where u_s is the sampling volume and ΔD is the resolution in drop diameter. Equation (32) shows that $\sigma/\overline{F}(X)$ is expected to exceed 1 when $u_s N_0^* \Delta D \overline{F}(X) \leq 1$. With $u_s = 0.15$ m^3, $N_0^* = 3 \times 10^6$ m^{-4}, and $\Delta D = 0.2$ mm, this is equivalent to $\overline{F}(X) \leq 1.45 \times 10^{-3}$, or $\log\overline{F}(X) \leq -2.83$. From Fig. 3g, this condition is fulfilled for $X > 1.5$. Thus, to explain the large fluctuations of the tail of the distribution it is not needed to invoke physical variability of the raindrop spectrum.

b. Results for convective rain

With the convective rain categories (Figs. 4–6), the normalized distribution $F(X)$ typically exhibits similar features as for stratiform. The tendency to bow shape

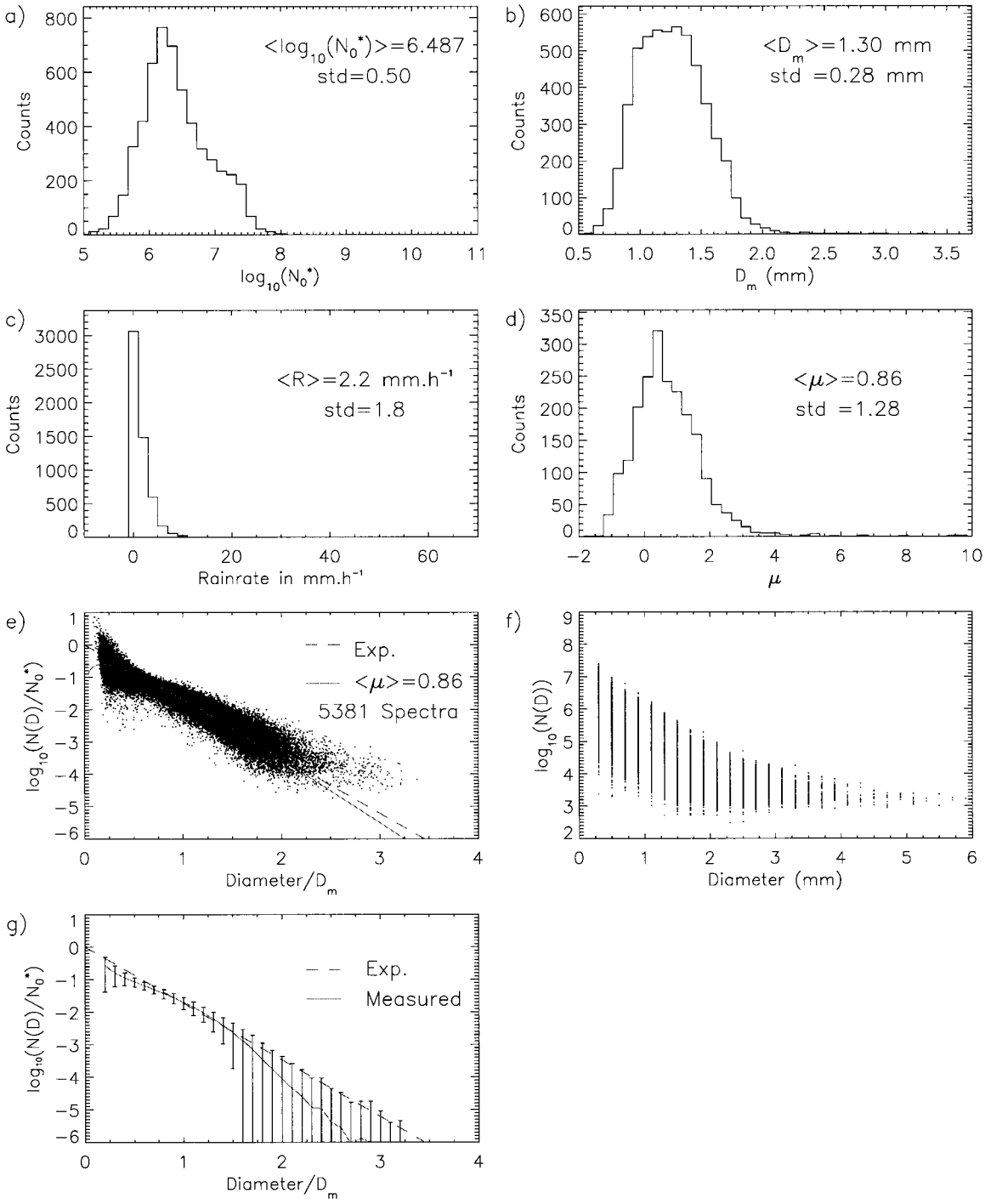

FIG. 3. Statistics for rain spectra classified as stratiform by the simple scheme. Histograms of (a) $\log(N_0^*)$, (b) D_m (mm), (c) R (mm h^{-1}), and (d) parameter μ of the best-fitting gamma distribution. (e) Overlay of all normalized spectra. (f) Overlay of all spectra without normalization. (g) Average and standard deviation of normalized spectra. In (e) and (g), the normalized shape for exponential DSD (dashed line) [and for gamma DSD (dotted line) in (e)] is shown for reference.

appears clearer and clearer from category C/0–10 to C/30–100. This identification of the shape is made possible by the normalization: without normalization (see Figs. 4f, 5f, and 6f), the scatter between the various spectra is much larger, and the bow shape is hardly identified. The progression of the average spectra $\overline{F}(X)$ and standard deviations among Figs. 4g, 5g, and 6g confirms that the DSD shape tends to be more and more stable as the rainfall rate increases, because the standard deviation decreases. The bow shape, particularly that for

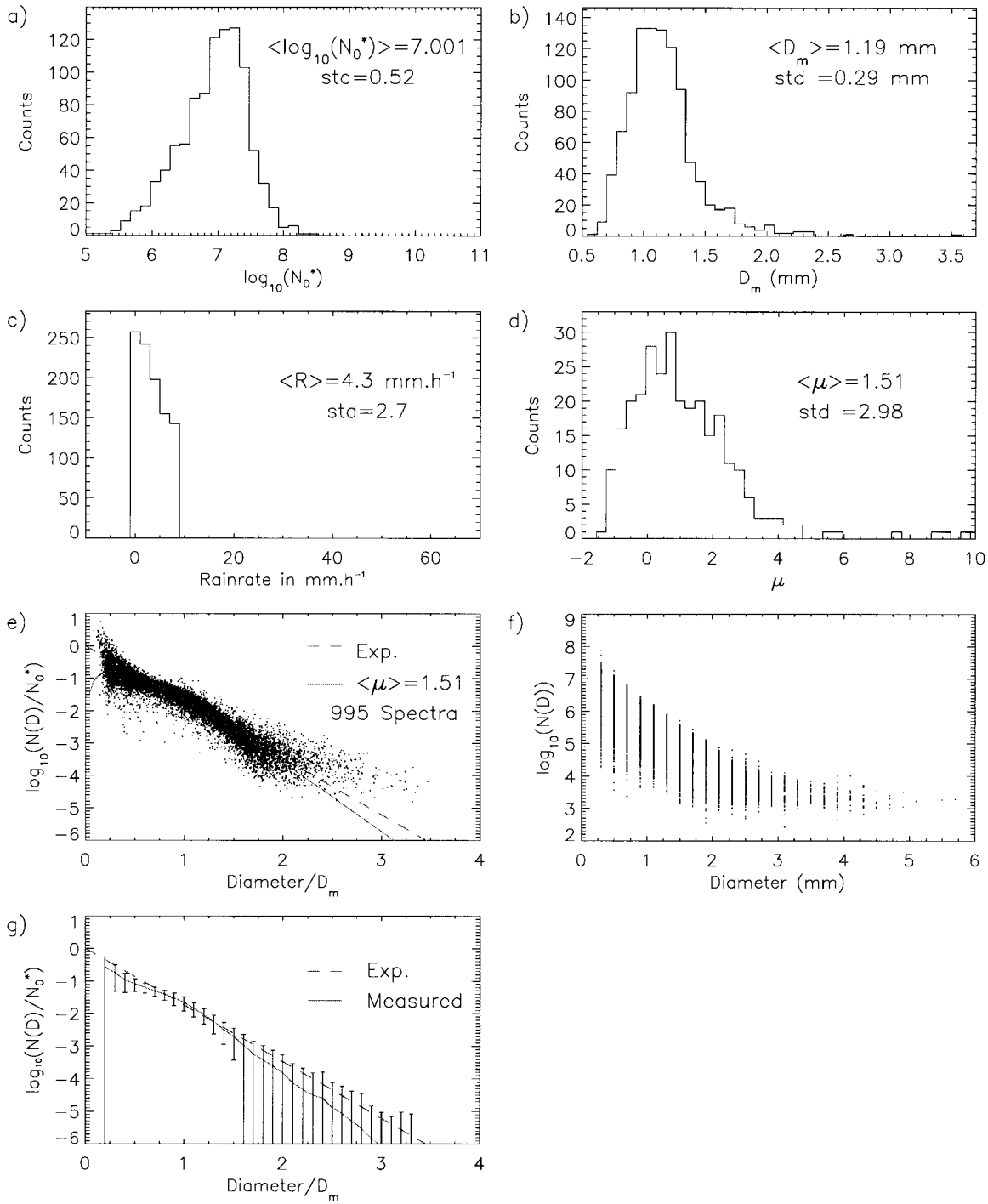

FIG. 4. Same as Fig. 3, but for rain spectra classified as convective by the simple scheme ($0 < R \leq 10$ mm h^{-1}).

C/30–100, is reminiscent of the Hu and Srivastava (1995) equilibrium distribution.

In the $\log(N_0^*)$ histograms, the three convective categories show a peak around 7.2. The histogram for category C/0–10 exhibits a left-side shoulder whose symmetry with the right-side shoulder of the stratiform category suggests that both are the result of misclassification. With the TS-type classification, both shoulders would disappear. Despite its probable imperfection, the simple criterion based on the 10-points series is nevertheless used in Figs. 3–6 because it is totally external to the N_0^* statistics. If the position of the peak of the $\log(N_0^*)$ histograms is about the same at the three convective rain categories, the peak of the highest rain-rate

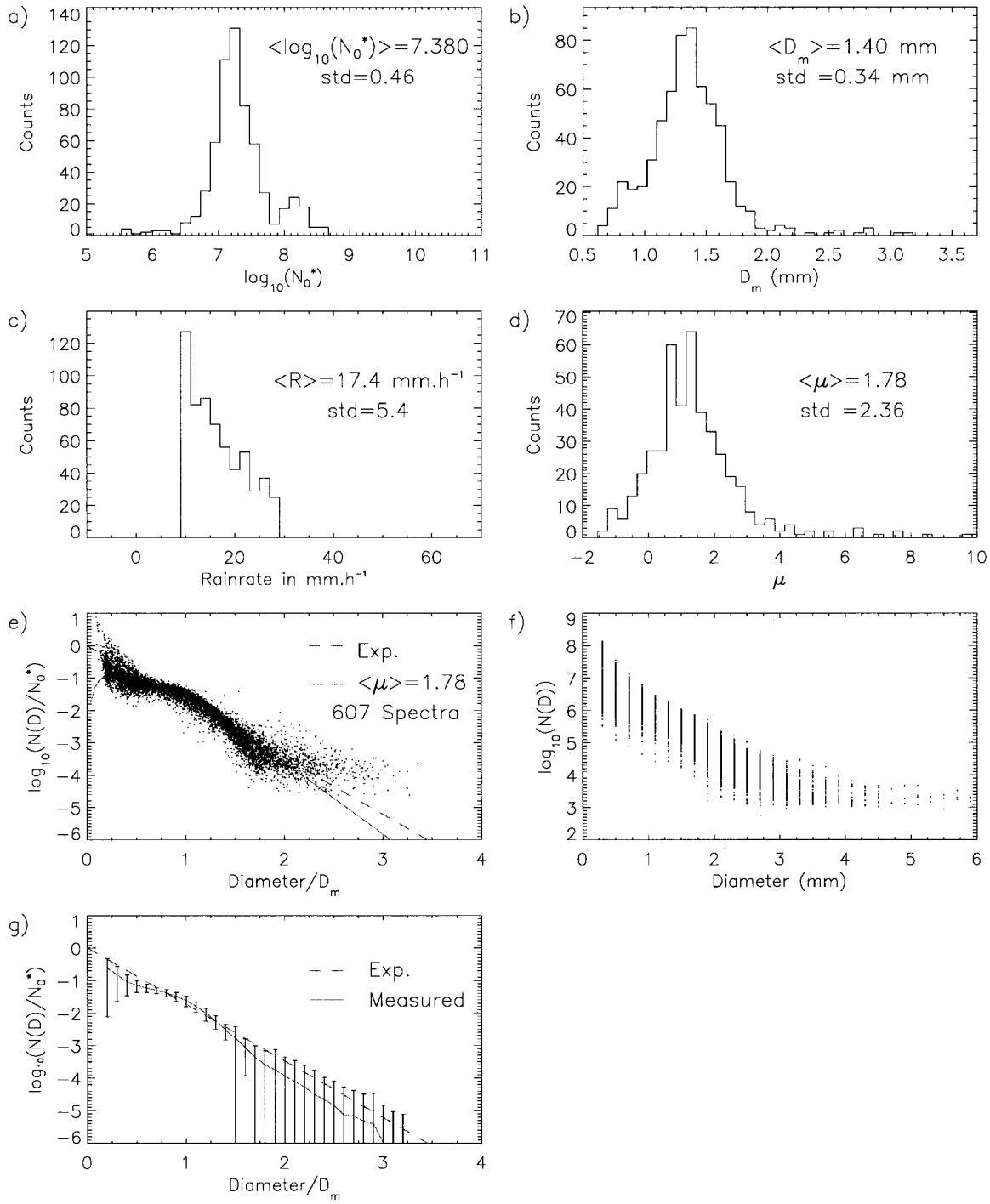

FIG. 5. Same as Fig. 3 , but for rain spectra classified as convective by the simple scheme ($10 < R \leq 30$ mm h^{-1}).

category C/30–100 seems to attract the largest percentage of counts, which manifests as a reduced standard deviation in $\log(N_0^*)$.

The D_m histograms extend over large intervals: 0.6–2.4 mm for category C/0–10, 0.6 to 3 mm for category C/10–30, and 0.9 to 3 mm for category C/30–100. A larger number of counts is concentrated at the main peak (1.6 mm) with category C/30–100.

The μ histograms do not show very distinct features between the three convective rain categories. Most spectra fall in the interval $-1 < \mu < +3$. This moderate variability is a net result of the numerical approach pres-

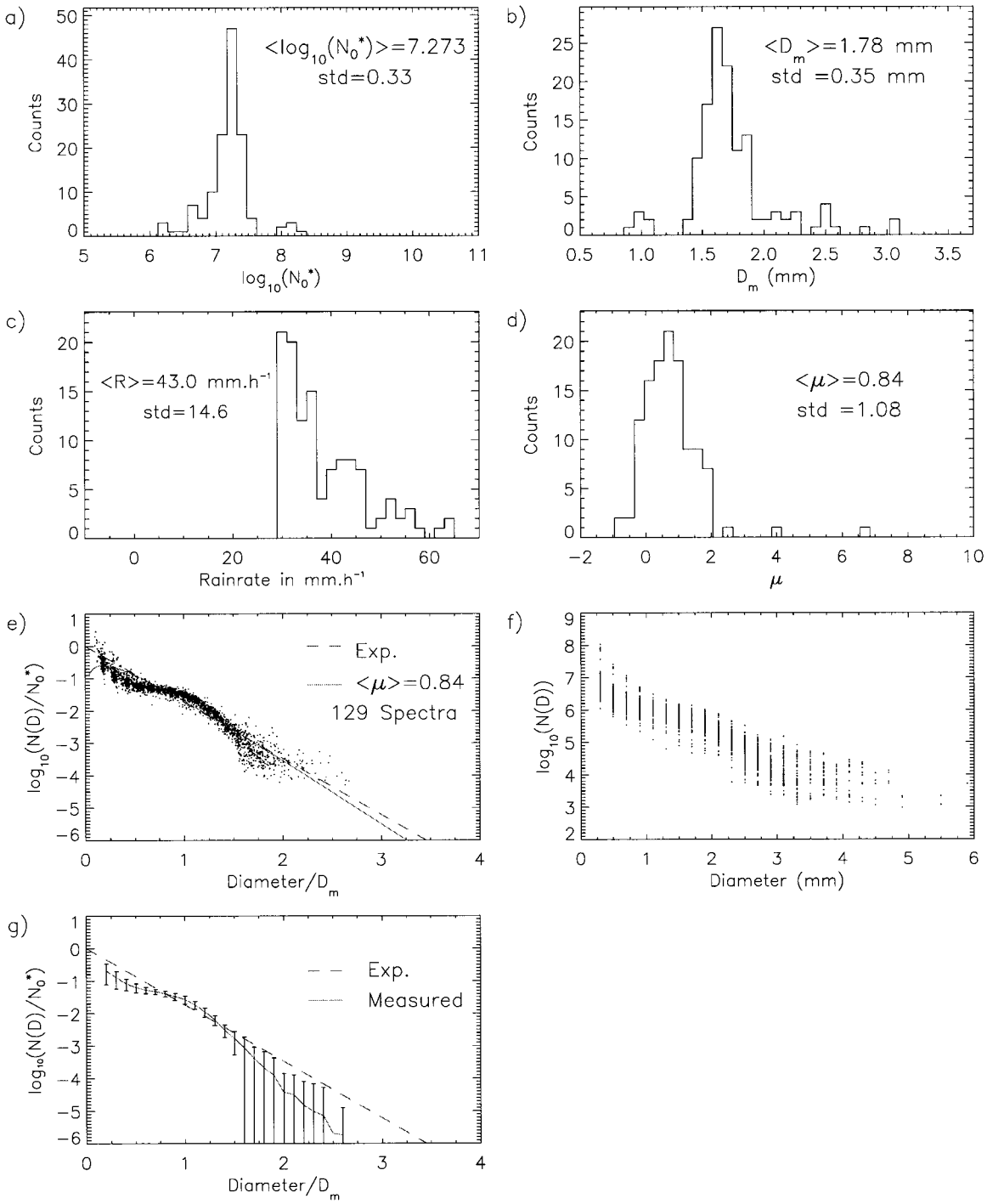

FIG. 6. Same as Fig. 3, but for rain spectra classifed as convective by the simple scheme ($30 < R \leq 100$ mm h^{-1}).

ently used to derive μ. When the method of moments as in Tokay and Short (1996) is applied to the current dataset, the same very large μ variability is obtained.

c. Comparison among the various rain categories

Table 3 synthesizes the characteristics of the N_0^*, D_m, R, and μ histograms presented in Figs. 3–6. It summarizes the mean and standard deviation of each parameter for each rain category. To appreciate whether the standard deviation in each histogram actually reflects physical variability or rather is due to the statistical fluctuations associated with drop counting, Table 4 displays the standard deviations in N_0^* and D_m expected from Poisson statistics. In Table 4, $\sigma(D_m)$ and

TABLE 3. Statistical characteristics of the various rain categories (S: stratiform; C: convective).

Rain category	log (N_0^*)		R (mm h^{-1})		D_m (mm)		Adjusted μ	
	Mean	Std dev	Mean	Std dev	Mean	Std dev	Mean	Std dev
S	6.487	0.50	2.2	1.8	1.3	0.28	0.86	1.28
C (0–10 mm h^{-1})	7.001	0.52	4.3	2.7	1.19	0.29	1.51	2.98
C (10–30 mm h^{-1})	7.380	0.46	17.4	5.4	1.4	0.34	1.78	2.36
C (30–100 mm h^{-1})	7.271	0.33	42.5	13.4	1.78	0.35	0.85	1.08

$\sigma[\log(N_0^*)]$ are calculated by introducing in (27) the means of D_m and N_0^* specified in Table 3. It can be seen that the standard deviations expected from the Poisson statistics (Table 4) are much smaller than those of the histograms (recalled in Table 3), especially when referring to categories C/10–30 and C/30–100. This result demonstrates that the dispersion of the D_m and N_0^* histograms in Figs. 3–6 actually reflects physical variability, not statistical error in the estimates.

For N_0^*, Table 3 confirms the distinct behavior of convective and stratiform rain spectra. However, the discrepancy between mean and ''peak'' values of $\log(N_0^*)$ in the case of categories S and C/0–10 is probably due to misclassification by the simple scheme. The best representative value for category S is possibly $\log(N_0^*) = 6.35$; it is $\log(N_0^*) = 7.20$ for category C/0–10. Whatever the rain category, the physical variability in $\log(N_0^*)$ is large, with standard deviations of ± 0.5 for S and C/0–10, ± 0.46 for C/10–30, and ± 0.3 for C/30–100. The mean volume diameter D_m also shows a large variability, with a standard deviation of ± 0.3 mm. It is interesting to note that the mean of D_m is larger for stratiform rain than for the first convective category C/0–10, despite the mean rainfall rate being smaller in S (2.2 mm h^{-1}) than in C/0–10 (4.3 mm h^{-1}). Among the three convective categories, D_m increases regularly, according roughly to $R^{1/4.67}$ as expected if N_0^* had a fixed value. From Table 3, there is no firm trend for μ among the various rain categories for the mean or for the standard deviation, and this result is consistent with the fact that the normalized shape is found stable between the various rain categories (see next section).

d. Overall statistical features of the DSD

Two features mark the overall statistics of the DSD from the TOGA COARE data, 1) a large variability of N_0^* and D_m, associated with a very weak correlation between these two parameters, and 2) a remarkable stability of the shape of the normalized DSD, whatever the rain category.

TABLE 4. Standard deviation in D_m and N_0^* expected assuming the Poisson distribution, for the various rain categories [from application of (27)].

Rain type	Standard deviation assuming Poisson distribution		
	$\sigma(D_m)$ (mm)	$\sigma(N_0^*)/N_0^*$ (%)	$\sigma[\log(N_0^*)]$
S	0.17	44.2	0.158
C (0–10 mm h^{-1})	0.091	25.35	0.125
C (10–30 mm h^{-1})	0.063	14.9	0.06
C (30–100 mm h^{-1})	0.081	15.1	0.06

1) VARIABILITY OF N_0^* AND D_M

Figure 7 displays the scatterplots of R versus D_m, R versus N_0^*, and N_0^* versus D_m, respectively, for the full dataset. The distinction between convective and stratiform spectra by the TS-type classification is also visualized. The variability of R and N_0^* covers three orders of magnitude, whereas that of D_m ranges from 0.6 to 2.2 mm (with a few extremes at 3 mm). These three scatterplots show qualitatively how weak the correlation is between R and D_m, R and N_0^*, N_0^* and D_m, respectively, when no distinction is made between stratiform and convective spectra. In contrast, Fig. 7d illustrates the current two-parameter parameterization. Because R is proportional to $\xi_{3.67} N_0^* D_m^{4.67}$ and $\xi_{3.67}$ is strongly constrained by the nearby moments ξ_3 and ξ_4, by definition equal to $\Gamma(4)/4^4$, it is not surprising that R/N_0^* is a near-perfect functional relationship of D_m.

The qualitative impression produced by Figs. 7a–c is confirmed in Table 5, which displays the linear correlation coefficient ρ^2 between $\log(R)$ and $\log(D_m)$, $\log(N_0^*)$ and $\log(R)$, and $\log(N_0^*)$ and $\log(D_m)$, calculated for various data subsets: 1) isolating the 14 December 1992 flight or considering all flights together, and 2) distinguishing stratiform and convective spectra (using the TS-type classification) or considering spectra of both categories together (referred to as ''all together''). Table 5 also gives the exponent of the best-fitting power-law relationships between R and D_m, N_0^* and R, and N_0^* and D_m. When no distinction is made between stratiform and convective, the correlation coefficient is always lower than 0.5. Because the current linear correlation coefficient addresses log quantities, any ρ^2 below 0.5 should be considered to be very low. The largest coefficient, $\rho^2 = 0.44$ (or 0.47 for the 14 December flight), is obtained for the N_0^*–R relationship: a power law such as $N_0^* \propto R^{1.31}$. After distinguishing between stratiform and convective, the correlation coefficient between N_0^* and R or N_0^* and D_m collapses to a value close to zero (thus the exponents of the corresponding power law are not significant), but that between R and D_m increases, reaching for convective rain $\rho^2 = 0.60$ and for the particular subset ''14 December 92—convective'' $\rho^2 = 0.88$. For this last subset, the power-law fit between R and D_m is

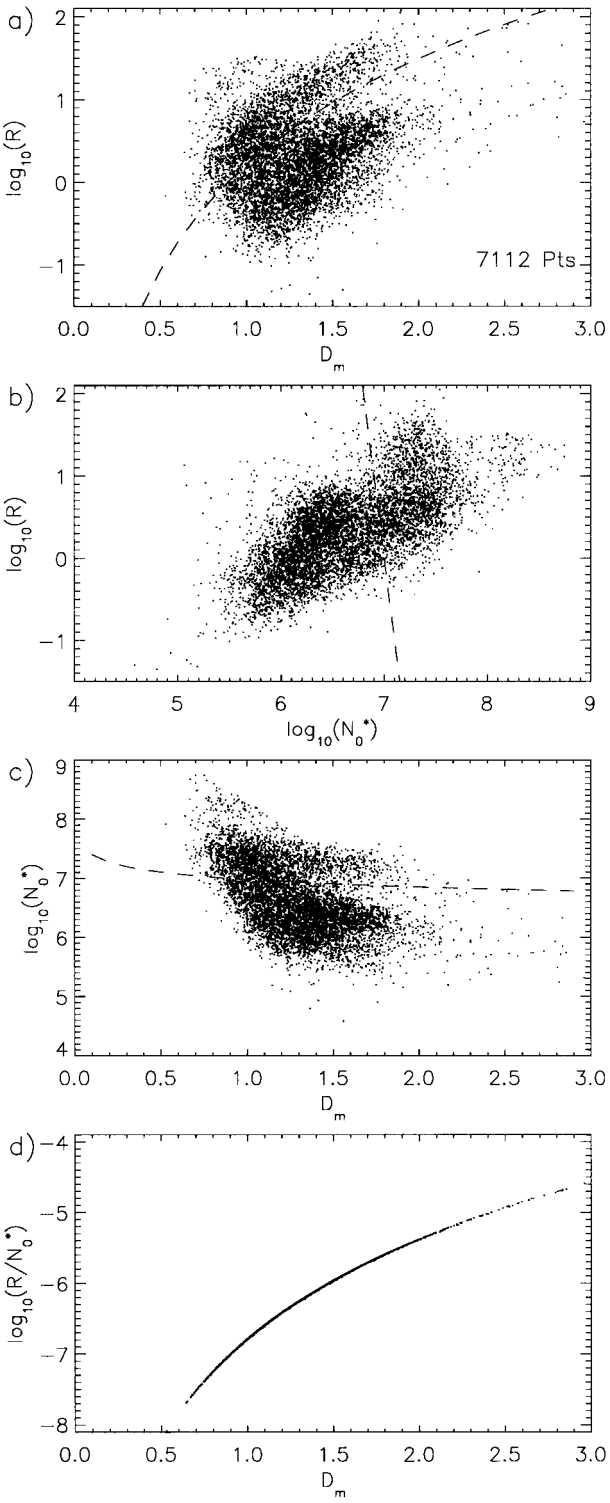

FIG. 7. For the entire TOGA COARE dataset, scatterplot of (a) $\log(R)$ vs D_m, (b) $\log(R)$ vs $\log(N_0^*)$, (c) $\log(N_0^*)$ vs D_m, and (d) $\log(R/N_0^*)$ vs D_m. Dashed lines visualize the criterion for Tokay and Short–type classification (see text).

$R \propto D_m^{4.11}$, close to the relationship $R \propto D_m^{4.67}$ expected with a constant value of N_0^*.

This statistical independence of N_0^* from R and D_m, after classification, is consistent with the picture from the previous section of an N_0^* affected by large variability but with a mean value by class of rainfall rate (for convective spectra) independent of R. The significant correlation between R and D_m obtained for convective spectra agrees with the trend for D_m to increase with R, as shown in Table 3. The relatively high correlation ($\rho^2 = 0.88$) obtained for the ''14 December 92'' flight for convective rain spectra and the exponent of the corresponding R–D_m power law close to 4.67 show that, within a specific event, N_0^* tends to be invariant. The variability of N_0^* from one event to the other explains the degradation of the correlation when the full dataset is considered. The relationship $N_0^* \propto R^{1.30}$ obtained for the full dataset, with very low correlation coefficient $\rho^2 = 0.44$, is only due to the association of low-rain-rate stratiform N_0^*s centered on $10^{6.2}$ with high-rain-rate convective N_0^*s centered on $10^{7.25}$.

Overall, the large variability of N_0^* and the quasi-absence of correlation between N_0^* and D_m illustrate the limits of the parameterizations of rain based on a single parameter [as in Marshall and Palmer (1948) or Sempere Torres et al. (1998)] that imply prescribed N_0^* or functional relationships between N_0^* and D_m, R and D_m, and R and N_0^*, respectively.

2) STABILITY OF THE DSD SHAPE

This second feature is illustrated in Fig. 8b, which compares the average normalized DSD $F(X)$ for the various rain categories. As expected, the average estimates are not as noisy as the individual normalized spectra, because averaging reduces the standard deviation by $n^{-0.5}$ (n: number of samples). What is striking is how close to one another the average normalized DSDs are for the four categories, despite the variety of rain type and rainfall-rate ranges. This is especially true for normalized diameter X less than 2, where the accuracy of the estimate is the best. Stratiform rain is produced from cloud water over a long time cycle from ice microphysical processes, whereas convective rain, particularly in the tropical oceanic convection of TOGA COARE, is dominated by short-cycle warm microphysics, that is, a direct conversion of the cloud water produced in the updraft into rain. It is surprising that such different formation mechanisms give rise to the same normalized DSD shape. This result suggests that a dominant physical mechanism (coalescence + breakup?) constrains the shape of the DSD even at low rainfall rate toward a ''universal'' shape.

To emphasize the interest of the normalization procedure, Fig. 8a displays, for reference, average spectra obtained from a ''classical'' averaging over all spectra belonging to each rain category. To make meaningful comparison with Fig. 8b, these average spectra have

TABLE 5. Linear correlation coefficient ρ^2 between log(R) and log(D_m), between log(N_0^*) and log(R), and between log(N_0^*) and log(D_m), and corresponding exponent of the power law between R and D_m, between N_0 and R, and between N_0^* and D_m for all the TOGA COARE rain spectra classified as stratiform, convective, or all together. Values for a subset corresponding to the 14 Dec 1992 flight are also shown. Boldface indicates statistical significance.

TOGA COARE data subset	R–D_m relationship		N_0^*–R relationship		N_0^*–D_m relationship	
	ρ^2	b of $R = aD_m^b$	ρ^2	b of $N_0^* = aR^b$	ρ^2	b of $N_0^* = aD_m^b$
Stratiform						
14 Dec 1992	0.39	3.29	0.30	2.22	0.1	−1.38
All flights	0.39	3.02	0.22	2.48	0.16	−1.65
Convective						
14 Dec 1992	**0.88**	**4.12**	0.00	0.01	0.12	−0.56
All flights	**0.61**	**3.43**	0.06	0.17	0.17	−1.25
All together						
14 Dec 1992	0.08	1.53	0.47	1.31	0.26	−3.14
All flights	0.07	1.40	0.44	1.31	0.30	−3.28

then been normalized. Thus the difference between Figs. 8a and 8b is only the order in which the two operations of ''normalization'' and ''averaging'' are performed. It is seen in Fig. 8a that the average spectra of the four categories are very close to exponential, and the corresponding log(N_0^*) is 6.57 for category S, 7.07 for C/0–10, 7.40 for C/10–30, and 7.24 for C/30–100. In a way, we refound the well-known result of previous authors (e.g., Marshall Palmer 1948; Joss and Gori 1978): when averaging numerous spectra belonging to a class of rainfall rates, one always obtains a raindrop spectrum close to the exponential. Thus the preliminary normalization of individual spectra is the only way to reach the ''true shape'' of the DSD.

Note also that, if the universal shape depicted in Fig. 8b departs significantly from the exponential [represented by exp(−4X)], it cannot be approximated by a gamma shape or a lognormal distribution, because these analytical shapes automatically associate a deficit of small drops to the convexity of the tail of the DSD. The following mathematical formulation is proposed instead, referred to in the following as ''modified exponential'':

$$F(X) = \exp[a - 4X - s\sqrt{(X - X_0)^2 + b}], \quad (33)$$

where the two parameter s (''slope'') and b (''smoothness'') may be fixed a priori, while the other two, a and X_0, have to be determined from the first two to verify $\xi_3 = \xi_4 = \Gamma(4)/4^4$. Good combinations suitable for the TOGA COARE data (illustrated in Fig. 8c) are 1) $s = 1.5$, $b = 0.06$, $X_0 = 1.124$, and $a = 0.705$ (referred to as modified exponential 1) and 2) $s = 2$, $b = 0.06$, $X_0 = 1.111$, and $a = 0.912$ (referred to as modified exponential 2). The corresponding form of $N(D)$ is

$$N(D) = N_0^* \exp\left[a - 4\frac{D}{D_m} - s\sqrt{\left(\frac{D}{D_m} - X_0\right)^2 + b}\right]. \quad (34)$$

Useful normalized moments for modified exponential 1 are

$$\xi_0 = 0.135\,25, \qquad \xi_{3.67} = 0.023\,441, \quad \text{and}$$
$$\xi_6 = 0.034\,995. \quad (35)$$

The great stability of the normalized shape $F(X)$, combined with the large variability and weak correlation of D_m and N_0^*, demonstrates that measurement of two integral parameters of the DSD is a *necessary and sufficient* condition to perform a good rain-rate retrieval.

6. The potential of N_0^* and D_m to parameterize rain relations

Because the shape of the DSD was found to be stable, two parameters suffice for its description: N_0^* and D_m. This section first argues about the interest of using N_0^* rather than D_m to parameterize the rain relations. Then it presents a verification that rain relations parameterized by N_0^* (or D_m) are much less dispersed than standard relationships, and it justifies their use in rain retrieval algorithms for dual-parameter radars.

a. *Pertinence of the parameterizations of rain by N_0^* or D_m*

To establish the power-law relationships between moments [(23)], D_m was arbitrarily eliminated between two moments M_i and M_j expressed by (21). It is also possible to eliminate N_0^* in order to establish a set of relationships parameterized by D_m as

$$M_i = \xi_i \xi_j^{-1} D_m^{i-j} M_j. \quad (36)$$

Thus, parameterization by D_m leads to a *linear relationship* between moments. From (36), the Z–R relationship (with the traditional assumption $R \propto M_{3.67}$) takes the form

$$Z = 140.4 \xi_6 \xi_{3.67}^{-1} D_m^{2.33} R. \quad (37)$$

Meanwhile, the parameterization by N_0^* implies [combining (24) and (25)]

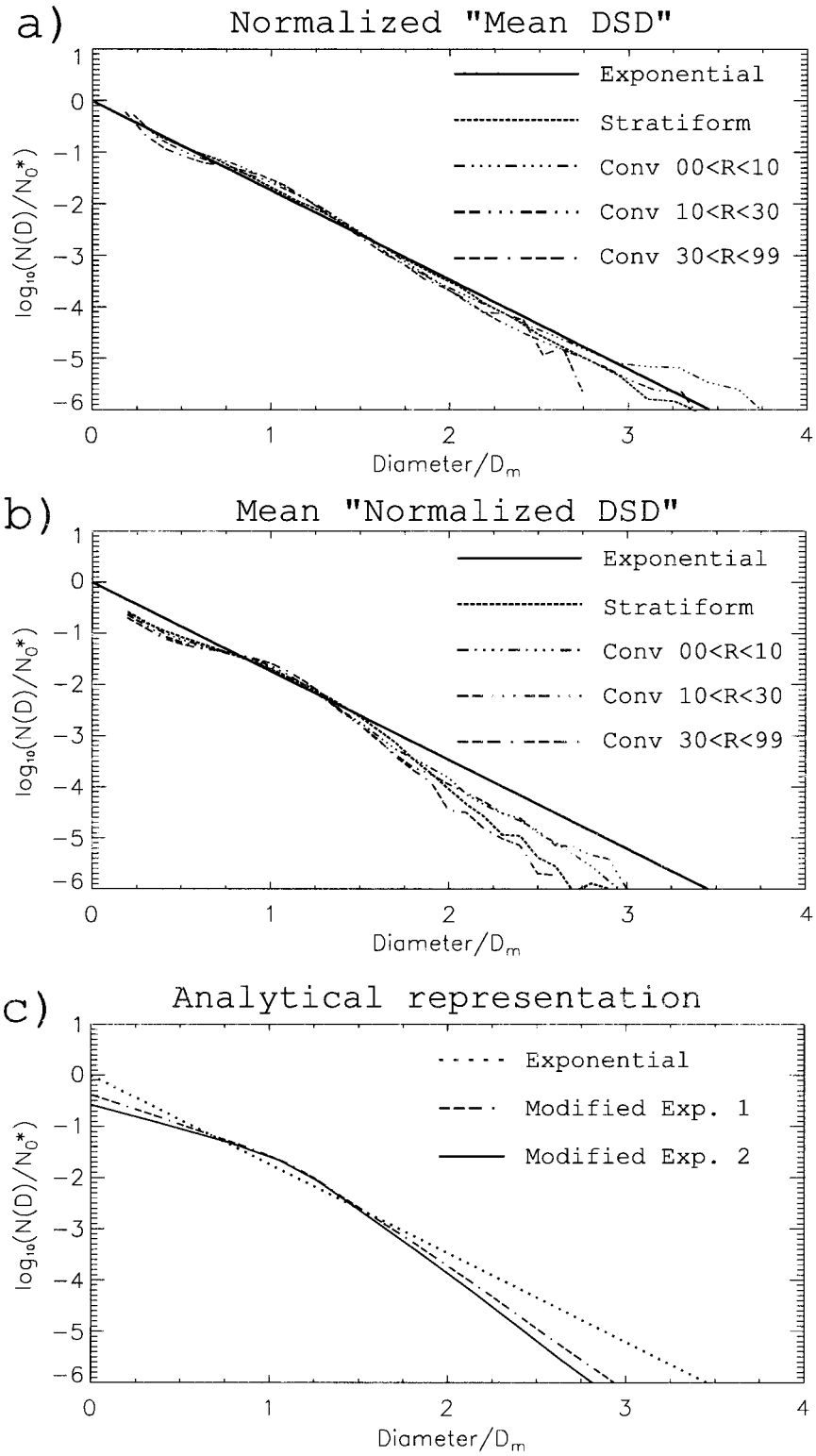

FIG. 8. (a) Normalized ''mean DSD'' for the various rain categories. (b) Mean ''normalized DSD'' for the various rain categories. (c) Analytical representation by (33) for $\{s = 1.5; b = 0.06\}$ (modified exp. 1) and $\{s = 2; b = 0.06\}$ (modified exp. 2).

$$Z = 5.2 \times 10^4 \xi_6 \xi_{3.67}^{-1.5} N_0^{*(-0.5)} R^{1.5}. \quad (38)$$

Mathematically, the two parameterizations are equally valid. Nevertheless they are not identical for the obvious reason that one is expressed with respect to N_0^* and the other to D_m, two independent parameters of the DSD. Equations (37) and (38) tell us that to estimate Z from R properly, a parameter of the DSD should also be known, either D_m in (37) or N_0^* in (38). The two parameterizations coincide only when an *extra relationship* is specified [as $N_0^* =$ constant, or $D_m =$ constant, or any function as $N_0^*(D_m)$, $N_0^*(R)$, or $D_m(R)$], which reduces the degrees of freedom from two to one. But all the sense of this paper is to show, *from the data*, that in the general case *no extra relationship* applies.

Though recognizing the equal validity of the two parameterizations, this paper favors the parameterization by N_0^* for two reasons:

1) *Mathematical*. In the general case, the integral parameters are not exact moments of the DSD: the rainfall rate R when the terminal velocity is not a power law of D as in Lhermitte (1988); the equivalent radar reflectivity Z_e and the specific attenuation when Mie scattering takes place, and so on. Nevertheless, it is always possible to normalize by N_0^*. Then universal relationships will be obtained between two normalized integral parameters, even if not power laws, as shown in Testud et al. (2000). Meanwhile the normalization by D_m^i is only valid when the integral parameters are *exact* moments of the DSD.
2) *Physical*. Though affected by a large variability, N_0^* adopts a *stationary* value with respect to R, distinct according to rain type (stratiform or convective), but D_m, at least for convective spectra, is observed to increase systematically with R. Moreover, within a specific event and after isolating convective rain spectra, N_0^* tends to behave as an invariant, but D_m increases with R approximately according to $R \propto D_m^{4.67}$ (i.e., as expected at constant N_0^*).

b. The TOGA COARE rain relations

Figure 9 displays the scatterplots for the full TOGA COARE dataset (without distinction of rain categories) between K and Z_e, between Z_e and R, and between K and R, before and after normalization of these three parameters by N_0^*. Here, K and Z_e are calculated from a Mie-scattering routine at the frequency of the Tropical Rainfall Measuring Mission (TRMM) precipitation radar, 13.8 GHz, described in Kummerow et al. (2000), and at 10°C. Table 6 displays the corresponding coefficients of best-fitting power laws and associated linear correlation coefficient ρ^2. Before normalization, the dispersion of the scatterplots in Fig. 9 is large, particularly for K–Z_e and R–Z_e. The K–R scatterplot is less dispersed, because K and R are associated with moments of the DSD of similar order, but the scattering spreads nevertheless over several decibels. After normalization of the three parameters by N_0^*, the dispersion of the scatterplots is considerably reduced, and the data points become organized along a straight line. The residual dispersion after normalization for the K–Z_e and R–Z_e relationships is on the order of ± 1 to 2 dB. This amount of dispersion seems appreciable. However, it should be kept in mind that the typical statistical uncertainty in Z_e *due to raindrop counting* is about ± 1.75 dB (see Table 2). Therefore, there is no need to invoke any physical variability in the shape of the DSD to explain this residual dispersion.

Table 6 shows that another way to reduce the scatter of the K–Z_e, K–R, and R–Z_e relationships is *classification* of rain type. When stratiform and convective raindrop spectra (sorted according to TS-type classification) are treated separately, distinct relationships are obtained, and the linear correlation coefficient ρ^2 gets closer to 1, nevertheless without reaching the degree of excellence of that obtained with normalized integral parameters. The case of the R–Z_e relationship is particularly significant in this respect: ρ^2 rises from 0.84 for the full dataset to 0.90 for the stratiform spectra subset, and to 0.92 for the convective one. Meanwhile, the normalized relationship allows achieving $\rho^2 = 0.98$. The improvement of the model of R–Z_e relationship through classification or normalization should be appreciated considering that the standard deviation with respect to the adjusted power law is proportional to $(1/\rho^2 - 1)^{1/2}$ (also displayed in Table 6). Another noticeable feature in Table 6 is that the exponent of the power law after classification gets much closer to that of the normalized power law. Referring again to the R–Z_e relationship, the exponent is 0.72 for the full dataset, 0.63 for the stratiform, and 0.66 for the convective. From the comparison with the exponent for the normalized power law (0.63),

TABLE 6. Information for K–Z_e, R–Z_e, and R–K relationships at the radar frequency 13.8 GHz and 10°C, as derived from the TOGA COARE microphysical data. The quality of the fit is expressed by the linear correlation coefficient ρ^2. The standard deviation is proportional to $1/(\rho^2 - 1)^{1/2}$.

$K = aZ_e^b$	a	b	ρ^2	$(1/\rho^2 - 1)^{1/2}$
Convective	5.07×10^{-4}	0.780	0.968	0.182
Stratiform	3.55×10^{-4}	0.758	0.962	0.199
All together	2.88×10^{-4}	0.815	0.938	0.257
Normalized	1.07×10^{-5}	0.763	0.987	0.114
$R = cZ_e^d$	c	d	ρ^2	$(1/\rho^2 - 1)^{1/2}$
Convective	4.81×10^{-2}	0.659	0.920	0.294
Stratiform	2.55×10^{-2}	0.632	0.897	0.339
All together	1.85×10^{-2}	0.720	0.838	0.439
Normalized	1.16×10^{-4}	0.629	0.977	0.153
$R = pK^q$	p	q	ρ^2	$(1/\rho^2 - 1)^{1/2}$
Convective	30.0	0.860	0.984	0.127
Stratiform	20.3	0.853	0.977	0.153
All together	27.6	0.921	0.969	0.178
Normalized	1.48	0.826	0.996	0.063

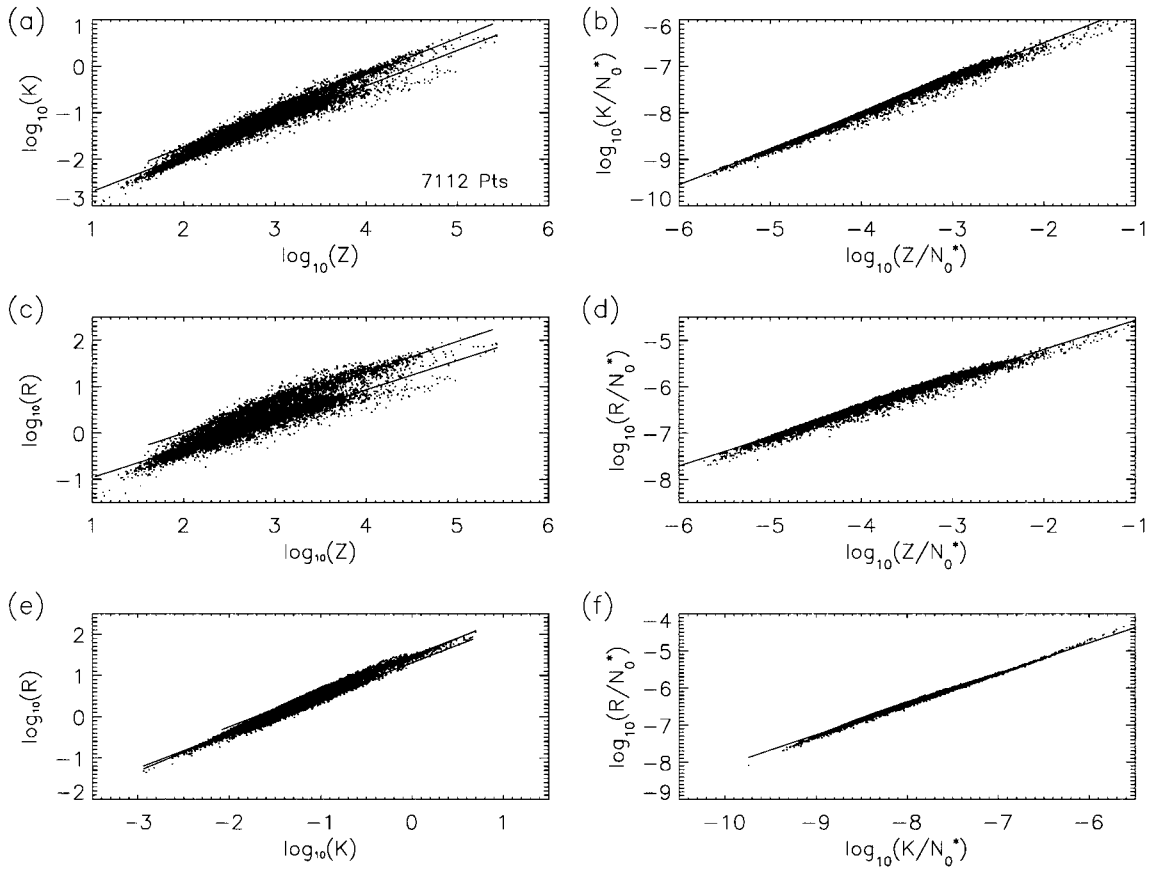

FIG. 9. The (a) (b) K–Z_e, (c) (d) R–Z_e, and (e) (f) R–K scatterplots (left) before and (right) after normalization by N_0^* for the full TOGA COARE dataset (Mie scattering calculation at 13.8 GHz and 10°C). The best-fitting power laws (defined in Table 6) are also shown 1) for convective and stratiform rain spectra, respectively, in the left diagrams and 2) for the full dataset of normalized parameters in the right diagrams.

we may infer that 1) the power law for stratiform rain corresponds to a constant N_0^* equal to 2.13×10^6 m^{-4} (in agreement with the peak value obtained in Fig. 3a) and 2) the power law for convective rain corresponds to N_0^* slowly varying with R as N_0^* equal to $1.24 \times 10^7 R^{0.12}$ (in reasonable agreement of the peak values displayed by Figs. 4a, 5a, and 6a).

When performed with $Z(=M_6)$ instead of Z_e, the analysis leads to the following results:

$$Z = 1.226R^{1.44} \quad \text{for convective} \quad (\text{with } \rho^2 = 0.94) \tag{39}$$

and

$$Z = 360.3R^{1.44} \quad \text{for stratiform} \quad (\text{with } \rho^2 = 0.92). \tag{40}$$

This result is in good agreement with the Z–R relationships derived for convective and stratiform rain by Tokay and Short (1996) from the disdrometer data collected at Kapingamarangi during TOGA COARE. They found

$$Z = 139R^{1.43} \quad \text{for convective} \quad \text{and} \tag{41}$$

$$Z = 367R^{1.30} \quad \text{for stratiform.} \tag{42}$$

c. Model verification

By introducing in (37) and (38) the normalized moments of the modified exponential shape defined in (35), one expects to obtain universal Z–R relationships parameterized by D_m and N_0^*, respectively. In Table 7, these theoretical relationships are compared with those empirically derived from linear regression on the full TOGA COARE dataset. The linear regression is operated between $\log(Z/D_m^{2.33})$ and $\log R$ to obtain the relationship parameterized by D_m. The agreement between theoretical and empirical relationships is very good for both parameterizations (by D_m and by N_0^*). In both cases, the exponent of the empirical relationship is very close to that expected from theory. The linear correlation coefficient ρ^2 reaches 0.9888 for the N_0^* parameterization and 0.9815 for the D_m one. Meanwhile, if a gamma DSD with $\mu = 1.25$ (average value for the four categories)

TABLE 7. The Z–R relationships parameterized by N_0^* and by D_m, as determined empirically (from the TOGA COARE dataset) or theoretically (with, as shape function, the modified exponential 1, or the gamma with $\mu = 1.25$).

Empirically derived (full TOGA COARE dataset)	$Z/N_0^* = 4.73 \times 10^{-5}(R/N_0^*)^{1.494}$ (with $\rho^2 = 0.9888$)	$Z = 204{D_m}^{2.33}R^{1.026}$ (with $\rho^2 = 0.9815$)
Theoretical (with modified exponential 1)	$Z/N_0^* = 4.87 \times 10^{-5}(R/N_0^*)^{1.499}$	$Z = 210{D_m}^{2.33}R$
Theoretical (with gamma, $\mu = 1.25$)	$Z/N_0^* = 5.64 \times 10^{-5}\ (R/N_0^*)^{1.499}$	$Z = 243{D_m}^{2.33}R$

is considered instead of the modified exponential, the agreement is not as good, the theoretical relationships leading to an overestimation of 20% (or 0.8 dBZ). From the theoretical relationship $Z = 210{D_m}^{2.33}R$, List's (1988) linear Z–R relationship $Z = 742R$ is obtained for $D_m = 1.72$ mm, which is approximately the value that was inferred to build Fig. 10.

d. Practical exploitation of the rain relations parameterized by N_0^* or D_m

With a classical radar, the classification of rain between stratiform and convective and subsequent application of distinct Z–R relationships has been recognized for a long time as a way to improve rain estimates. It was shown in the previous sections that the rain relations parameterized by N_0^* are much less dispersed that those for stratiform or convective rain, which demonstrates the potential improvement that could be achieved using a two-parameter radar, such as dual frequency or dual polarization. In a sense, the TRMM precipitation radar may also be considered to be ''dual parameter,'' because in addition to the attenuated reflectivity profile, it allows deriving the total path attenuation from the return of the surface used as a reference target. Among the rain retrieval algorithms available to exploit dual-parameter radar data, *profiling algorithms* [as described by Kozu and Nakamura (1991), Marzoug and Amayenc (1994), and Testud et al. (2000)] are of particular interest because of their great numerical stability. However, this stability is paid for by the assumption of some invariant along the integration path. In Ferreira and Amayenc (1999), Testud et al. (2000), and Le Bouar et al. (2001), parameter N_0^*, which is assumed to be invariant along the path, may be retrieved by the algorithm, and its estimate is subsequently used to scale all the rain relations and to achieve an improved R estimate. With an S-band polarimetric radar, the measurement of the differential reflectivity ZDR gives an estimate of D_m, thus in an algorithm combining Z and ZDR the *linear* relationship parameterized by D_m should be preferred.

7. Discussion in respect to equilibrium theory

This section aims at investigating to what extent the DSD characteristics described in section 5 are compatible with the equilibrium theory. The concept of equilibrium distribution, or distribution reached when the processes of coalescence and breakup dominate the others (e.g., nucleation, diffusion growth, evaporation, sedimentation, advection), has been investigated by Valdez and Young (1985), Brown (1986), List et al. (1987), and Hu and Srivastava (1995). All of these studies converge to say that 1) the characteristic time to reach equilibrium is inversely proportional to the rainfall rate (Srivastava 1988) and 2) the equilibrium solution consists of a family of DSDs proportional to one another that may be

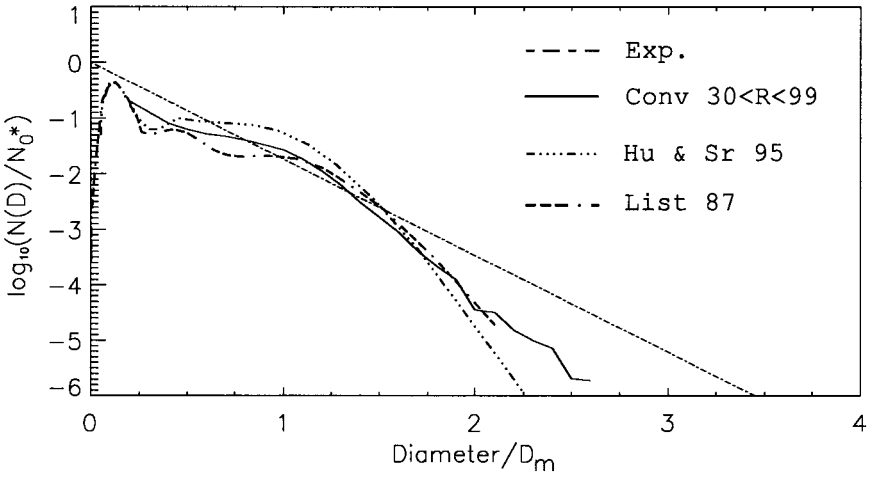

FIG. 10. Comparison of the theoretical equilibrium distributions calculated by Hu and Srivastava (1995) and List et al. (1987) with the mean normalized DSD for convective rain (30–100 mm h^{-1}). The theoretical DSD has been normalized in the same way as the experimental ones ($D_m \approx$ 1.75 mm applies to both theoretical DSDs).

TABLE 8. Mean values of rainfall rate, N_0^*, D_m, and total concentration n_T for three subcategories of intense convective rain.

Rain category	No. of spectra	$\overline{R}$ (mm h^{-1})	$\overline{N_0^*}$ (m^{-4})	$\overline{D_m}$ (mm)	$\overline{n_T}$ (m^{-3})
C (30–40 mm h^{-1})	72	33.8	2.13×10^7	1.65	4.75×10^3
C (40–50 mm h^{-1})	31	44	1.82×10^7	1.80	4.43×10^3
C (50–100 mm h^{-1})	25	65.3	1.32×10^7	2.11	3.77×10^3

described as $N(D) = R\psi(D)$, where $\psi(D)$ is a generic shape function (List et al. 1987).

The typical time to reach equilibrium, starting from a Marshall–Palmer or lognormal DSD, is a few minutes at 100 mm h^{-1}, a few tens of minutes at 10 mm h^{-1}, and two hours at 1 mm h^{-1}. Because the time for a raindrop to drop from 3000 m is about 10 min, the equilibrium theory seems a priori irrelevant for R less than 30 mm h^{-1}. Thus the current comparison is focused mainly on the raindrop spectra from convective rain category C/30–100. Figure 10 compares the average normalized distribution $F(X)$ for category C/30–100 with the *normalized* equilibrium distributions $F_{eq}(X)$ derived from the modeling studies by Hu and Srivastava (1995) and List et al. (1987). The agreement is good.

More difficult to explain is the fact that the model-derived $F_{eq}(X)$s are also close to the $F(X)$s of the other rain categories (because they are very close to one another, as shown in Fig. 8b). At the lowest rain rates, the collision coalescence–breakup kernel is a *weak attractor* toward the equilibrium DSD, but if the initial DSD is not too far from equilibrium its action could suffice to maintain the DSD shape close to equilibrium. The case of the stratiform rain category is particularly puzzling: at such low rain rates, there is very little drop interaction. For the stratiform rain layer, the ''initial'' DSD is the DSD just below the bright band, which is a direct image after melting of the ice particle distribution aloft (Zawadzki et al. 1994). Why should this initial DSD, resulting from the precipitation growth in ice phase, be close to equilibrium?

For rain category C/30–100 for which the confrontation with equilibrium theory should not be subject to restriction, in addition to the shape of the DSD, another point of agreement is the mean value of D_m, near 1.78 mm in Table 3. A similar D_m value (1.75 mm) can be estimated from Hu and Srivastava's and List et al.'s equilibrium DSD. Nevertheless Table 8 demonstrates that this last point of agreement is only apparent. After dividing C/30–100 into three sub categories C/30–40 (72 spectra), C/40–50 (31 spectra), and C/50–100 (25 spectra), it is realized that D_m, expected to be an invariant according to the equilibrium theory, regularly increases with R. Meanwhile, N_0^*, expected to increase proportionally to R, in fact decreases slowly. From Table 8, the best invariant, if any, may be the total number of particles n_T, itself expected to increase proportionally to R from equilibrium theory.

Discrepancy of the observations with theory also lies in the large variability of N_0^* and D_m, well beyond statistical errors (already commented on in section 5b,c). Such a variability, combined with the fact that the ''equilibrium shape'' is obtained only after normalization of observed spectra (see Figs. 8a,b), tends to show that the equilibrium solutions could be a twofold variety: *scaling by drop diameter* would have to be considered in addition to scaling by concentration. In the same line, it is interesting to recall that Zawadzki and Agostinho Antonio (1988), in their analysis of raindrop spectra from intense tropical rain in Brazil, showed the existence of natural DSDs compatible with the equilibrium theory, that is, well described by the shape function $\psi(D)$ of Valdez and Young (1985) or List et al. (1987). But they also reported about DSDs for high rainfall rate (50–150 mm h^{-1}) that should correspond to *another* equilibrium with a different shape function characterized by much higher concentration of large drops. After correcting these DSDs for the deficit of small raindrops (a usual instrumental effect with disdrometers), this ''other equilibrium'' possibly reduces to ''another D_m,'' larger than that predicted by equilibrium theory.

8. Conclusions

The concept of normalization of the particle size distribution developed in this paper is similar to those of Sekhon and Srivastava (1971), Willis (1984), Sempere Torres et al. (1998), Dou et al. (1999), Testud et al. (2000), and Uijlenhoet (1999). As in Sekhon and Srivastava (1971), Willis (1984), and Testud et al. (2000), this normalization is founded upon two reference variables, the liquid water content and, in this new concept, the mean volume diameter D_m (easier to manipulate than the median volume diameter D_0). From a mathematical analysis free of *any assumption* about the shape of the DSD, it was established that, to identify a shape *independent* of LWC and D_m, the scaling parameters of the drop size distribution $N(D)$ should be $N_0^* \propto \mathrm{LWC}/D_m^4$ with respect to concentration, and D_m with respect to drop diameter. Here, N_0^* may also be defined as the intercept parameter that an exponential DSD with the same LWC and D_m as the real one would have. With this normalization, two moments of the DSD M_i and M_j are related by a power law parameterized by N_0^*.

This new normalization has been applied to the ensemble of the TOGA COARE airborne microphysical data. Under the assumption that the drop counting obeys Poisson statistics, it is possible to estimate the uncertainty in N_0^* and D_m calculated by the method of moments. On the full dataset (7112 raindrop spectra collected during the 21 flights), the scatterplot of N_0^* versus

D_m is heavily dispersed, and this dispersion is far beyond that expected from statistical errors.

The classification of the TOGA COARE raindrop spectra into four categories [one stratiform and three convective (0–10, 10–30, and 30–100 mm h^{-1})] allowed us to identify the following features:

1) There is a distinct behavior of N_0^* between stratiform and convective rains; a typical stratiform value is $2.2 \times 10^6\ m^{-4}$, whereas it is $2 \times 10^7\ m^{-4}$ in convective.
2) Between the convective rain categories, there is a clear trend for D_m to increase as the rainfall rate increases.
3) After classification, there is no correlation between N_0^* and R or between N_0^* and D_m.
4) The ''average'' normalized shape of the DSD is remarkably stable among the four rain categories.

The stability of the DSD normalized shape for the heavy convective rain category and its similarity to equilibrium distribution described by List et al. (1987) or Hu and Srivastava (1995) suggests that it is dominated by the collisional interaction of raindrops. However, there are important discrepancies between the results of this analysis and equilibrium theory: D_m shows a large variability, with a tendency to increase with R, although it is expected to be constant according to the theory; N_0^* does not show any correlation with R, whereas it should be proportional to R from the theory. The average normalized shapes from the various rain categories (stratiform, light convective, moderate convective, or heavy convective) are very close to one another, which is not easy to understand either, given that there is little drop interaction at low rain rate. Further studies are needed to understand if the discrepancy between equilibrium theory and the observations is due to the fact that most of the observations are ''out of equilibrium,'' or whether there is a problem with the equilibrium theory itself.

With respect to any practical application to the remote sensing of rain, the stability of the DSD normalized shape shows that two parameters, and only two, are needed to describe any DSD. With two degrees of freedom for the DSD, a relationship between moments parameterized by N_0^* (or D_m) is expected to be very robust. From the TOGA COARE airborne microphysical data, the current paper could verify that the rain relations (such as the Z–R relationship) are less dispersed after rain type classification (convective vs stratiform). In this respect, its results are similar to Tokay and Short's (1996), from the Kapingamarangi disdrometer data. However, it also showed that the normalization by N_0^* constitutes a much higher step in reducing the dispersion of rain relations. This justifies the development of dual-parameter radars (dual frequency or dual polarization, for example) associated with a profiling algorithm that is able to estimate N_0^* (as in Testud et al. 2000).

Acknowledgments. This research was supported in part by the U.S. National Science Foundation under a cooperative agreement with the University Corporation for Atmospheric Research and by the French Institut National des Sciences de l'Univers. Part of this work has been accomplished in the framework of the EuroTRMM project funded by the European Commission and European Space Agency.

APPENDIX

The Accuracy of the Method of Moments for Analyzing Measured Raindrop Spectra

a. Statistical uncertainty in drop counting in each diameter class

Let $l(D_i)$ be the number of drops counted by the microphysical probe in the diameter class centered on D_i and of width ΔD. Assuming a Poisson distribution, the average and variance of $l(D_i)$ are given by

$$\overline{l(D_i)} = u_s N(D_i)\Delta D \quad \text{and} \tag{A1}$$

$$\text{var}\{l(D_i)\} = u_s N(D_i)\Delta D, \tag{A2}$$

where u_s is the sampled volume.

Thus the variance in the estimate $\hat{N}(D)$ OF $N(D)$ is

$$\text{var}\{\hat{N}(D_i)\} = N(D_i)/(u_s \Delta D), \tag{A3}$$

and its relative standard deviation is

$$\sigma\{\hat{N}(D_i)\}/N(D_i) = [(u_s N(D_i)\Delta D]^{-1}. \tag{A4}$$

Considering that $F(X_i) = N(D_i)/N_0^*$, the relative standard deviation of the normalized DSD is

$$\sigma\{F(X_i)\}/F(X_i) = [u_s N_0^* F(X_i)\Delta D]^{-1}. \tag{A5}$$

b. Statistical error in the estimate of moments of the drop spectra

The estimate $\hat{M}_i$ of the moment of order i from the measured raindrop spectra is

$$\hat{M}_i = \sum_k D_k^i \hat{N}(D_k)\Delta D, \tag{A6}$$

where k indicates the diameter class. It follows that

$$\text{var}\{\hat{M}_i\} = \sum_k D_k^{2i}\ \text{var}\{\hat{N}(D_k)\}\Delta D^2 = u_s^{-1} \sum_k D_k^{2i} N(D_k)\Delta D. \tag{A7}$$

For this error calculation, $N(D)$ is assumed to be exponential:

$$N(D) = N_0 \exp(-4D/D_m). \tag{A8}$$

Replacing the summation by the integral in (A6) and (A7), it may be written that

$$\overline{\hat{M}_i} = M_i = \int_0^\infty D^i N(D)\, dD = N_0 D_m^{i+1}\Gamma(i+1)/4^{i+1} \quad \text{and} \tag{A9}$$

$$\text{var}\{\hat{M}_i\} = u_s^{-1}\int_0^\infty D^{2i}N(D)\, dD = u_s^{-1}N_0 D_m^{2i+1}\Gamma(2i+1)/4^{2i+1}. \tag{A10}$$

In terms of the relative standard deviation, (A10) may be rewritten

$$\sigma(\hat{M}_i)/M_i = 2(u_s N_0 D_m)^{-1/2}[\Gamma(2i+1)]^{1/2}/\Gamma(i+1). \tag{A11}$$

c. Correlation between estimates of moments

The probability average of the product of the two estimates $\hat{M}_i$ and $\hat{M}_j$ is expressed as

$$\overline{\hat{M}_i\hat{M}_j} = \overline{\left[\sum_k D_k^i \hat{N}(D_k)\Delta D\right]\left[\sum_k D_k^j \hat{N}(D_k)\Delta D\right]}, \quad \text{or} \tag{A12}$$

$$\overline{\hat{M}_i\hat{M}_j} = \overline{\left\{\sum_k D_k^i [N(D_k)+\delta N(D_k)]\Delta D\right\}\left\{\sum_k D_k^j [N(D_k)+\delta N(D_k)]\Delta D\right\}}, \tag{A13}$$

where $\delta N = \hat{N} - N$.

Because $\overline{\delta N(D_i)\delta N(D_j)} = 0$ when $i \neq j$, and $\overline{\delta N^2(D_k)} = \text{var}[\hat{N}(D_k)]$ [see (A3)], (A13) may be rewritten, replacing the summation by the integral

$$\hat{M}_i\hat{M}_j = M_i M_j + u_s^{-1}\int_0^\infty D^{i+j}N(D)\, dD. \tag{A14}$$

Thus,

$$\overline{\delta M_i \delta M_j} = u_s^{-1}M_{i+j}. \tag{A15}$$

By combining (A14) and (A8), it follows that the correlation between errors in $\hat{M}_i$ and $\hat{M}_j$ is expressed as

$$c_{ij} = \frac{\overline{\delta M_i \delta M_j}}{\sqrt{\overline{\delta M_i^2}\,\overline{\delta M_j^2}}} = \frac{\Gamma(i+j+1)}{\sqrt{\Gamma(2i+1)\Gamma(2j+1)}}. \tag{A16}$$

Note that c_{ij} is *independent* from the sampling volume u_s.

d. Errors in the estimates of N_0^* and D_m

In sections 4 and 5, N_0^* and D_m are calculated as

$$D_m = M_4/M_3 \quad \text{and} \tag{A17}$$

$$N_0^* = [4^4/\Gamma(4)]M_3^5 M_4^{-4}. \tag{A18}$$

Differentiation of (A17) brings

$$\delta D_m/D_m = \delta M_4/M_4 - \delta M_3/M_3. \tag{A19}$$

Thus,

$$\overline{\delta D_m^2}/D_m^2 = \overline{\delta M_4^2}/M_4^2 + \overline{\delta M_3^2}/M_3^2 - 2c_{34}\sqrt{\overline{\delta M_4^2}\,\overline{\delta M_3^2}}/(M_3 M_4). \tag{A20}$$

Similarly,

$$\overline{\delta N_0^{*2}}/N_0^{*2} = 16\overline{\delta M_4^2}/M_4^2 + 25\overline{\delta M_3^2}/M_3^2 - 40c_{34}\sqrt{\overline{\delta M_4^2}\,\overline{\delta M_3^2}}/(M_3 M_4). \tag{A21}$$

Taking account of (A9) and (A14), the relative standard deviations in D_m and N_0^* are

$$\frac{\sigma(D_m)}{D_m} = \frac{2}{\sqrt{u_s N_0^* D_m}}\left\{\frac{\Gamma(9)}{[\Gamma(5)]^2} + \frac{\Gamma(7)}{[\Gamma(4)]^2} - 2\frac{\Gamma(8)}{\Gamma(5)\Gamma(4)}\right\}^{1/2} \tag{A22}$$

and

$$\frac{\sigma(N_0^*)}{N_0^*} = \frac{2}{\sqrt{u_s N_0^* D_m}} \times \left\{16\frac{\Gamma(9)}{[\Gamma(5)]^2} + 25\frac{\Gamma(7)}{[\Gamma(4)]^2} - 40\frac{\Gamma(8)}{\Gamma(5)\Gamma(4)}\right\}^{1/2}. \tag{A23}$$

e. General form of the errors in N_0^*, D_m, LWC, R, and Z

The general form of the relative standard deviation expressed in (A11), (A22), and (A23) is the following

$$\sigma(P)/P = 2\gamma_p/(u_s N_0^* D_m)^{1/2}, \tag{A24}$$

where P represents any of the parameters N_0^*, D_m, LWC, R, or Z, and γ_p is the corresponding coefficient. Table A1 displays the values of γ_p.

TABLE A1. Coefficient γ_P of the relationship $\sigma(P)/P = 2\gamma_P/(\mu_s N_0^* D_m)^{1/2}$ attached to the five parameters of interest.

Parameter	N_0^*	D_m	LWC	R	Z
Coefficient γ_P	14.83	4.47	4.47	6.79	30.39

REFERENCES

Atlas, D., and C. W. Ulbrich, 1977: Path- and area-integrated rainfall measurement by microwave attenuation in the 1–3 cm band. *J. Appl. Meteor.*, **16**, 1322–1331.

——, ——, F. D. Marks Jr., R. A. Black, E. Amitai, P. T. Willis, and C. E. Samsury, 2000: Partitioning tropical oceanic convective and stratiform rains by draft strength. *J. Geophys. Res.*, **105,** 2259–2267.

Battan, L. J., 1973: *Radar Observation of the Atmosphere*. The University of Chicago Press, 324 pp.

Best, A. C., 1950: The size distribution of raindrops. *Quart J. Roy. Meteor. Soc.*, **76**, 16–36.

Brown, P. S., Jr., 1986: Analysis of the Low and List drop-breakup formulation. *J. Climate Appl. Meteor.*, **25**, 313–321.

Chandrasekar, V., and V. N. Bringi, 1987: Simulation of radar reflectivity and surface measurements of rainfall. *J. Atmos. Oceanic Technol.*, **4**, 464–478.

Dou, X.-K., J. Testud, and P. Amayenc, 1999: The parameterization of rain for a weather radar. *C.R. Acad. Sci. Paris*, **328**, 577–582.

Feingold, G., and Z. Levin, 1986: The log-normal fit to raindrop spectra from convective clouds in Israel. *J. Climate Appl. Meteor.*, **25**, 1346–1363.

Ferreira, F., and P. Amayenc, 1999: Impact of adjusting rain relations on rain profiling estimates from the TRMM Precipitation Radar. Preprints, *29th Conf. on Radar Meteorology*, Montreal, PQ, Canada, Amer. Meteor. Soc., 643–646.

Hauser, D., P. Amayenc, B. Nutten, and P. Waldteufel, 1984: A new optical instrument for simultaneous measurement of raindrop diameter and fall speed distribution. *J. Atmos. Oceanic Technol.*, **1**, 256–269.

Hu, Z., and R. C. Srivastava, 1995: Evolution of raindrop size distribution by coalescence, breakup, and evaporation: Theory and observations. *J. Atmos. Sci.*, **52**, 1761–1783.

Joss, J., and A. Walvogel, 1967: Ein Spektrograph für Niederschlag strophen mit automatisher auswertung (A spectrograph for automatic measurement of rainfall). *Geofis. Pura Appl.*, **68**, 240–246.

——, and E. G. Gori, 1976: The parametrisation of raindrop size distributions. *Rev. Ital. Geophys.*, **III N,** 275–383.

——, and ——,1978: Shapes of raindrop size distributions. *J. Appl. Meteor.*, **17**, 1054–1061.

Knollenberg, R. G., 1970: The optical array: An alternative to scattering or extinction for airborne particle size determination. *J. Appl. Meteor.*, **9**, 86–103.

——, 1981: Techniques for probing cloud microstructure. *Clouds, Their Optical Properties and Effects*, P. V. Hobbs and A. Deepak, Eds., Academic Press, 15–89.

Kozu, T., and K. Nakamura, 1991: Rainfall parameter estimation from dual-radar measurements combining reflectivity profile and path-integrated attenuation. *J. Atmos. Oceanic Technol.*, **8**, 259–270.

Kummerow C., and Coauthors, 2000: The status of the Tropical Rainfall Measuring Mission (TRMM) after two years in orbit. *J. Appl. Meteor.*, **39**, 1965–1982.

Law, J. O., and D. A. Parsons, 1943: The relation of raindrop size to intensity. *Trans. Amer. Geophys. Union*, **24**, 452–460.

Le Bouar, E., J. Testud, and T. Keenan, 2001: Validation of the rain profiling algorithm ''ZPHI'' from the C-band polarimetric weather radar in Darwin. *J. Atmos. Oceanic Technol.*, in press.

Lhermitte, R., 1988: Cloud and precipitation sensing at 94 GHz. *IEEE Trans. Geosci. Remote Sens.*, **29**, 690–703.

List, R., 1988: A linear radar reflectivity-rainrate relationship for steady tropical rain. *J. Atmos. Sci.*, **45**, 3564–3572.

——, N. R. Donaldson, and R. E. Stewart, 1987: Temporal evolution and drop spectra to collisional equilibrium in steady and pulsating rain. *J. Atmos. Sci.*, **44**, 362–372.

Low, T. B., and R. List, 1982a: Collision, coalescence and breakup of raindrops. Part I: Experimentally established coalescence efficiencies and fragment size distribution in breakup. *J. Atmos. Sci.*, **39**, 1591–1606.

——, and ——, 1982b: Collision, coalescence and breakup of raindrops. Part II: parameterization of fragment size distributions. *J. Atmos. Sci.*, **39**, 1607–1618.

Markowitz, A. H., 1976: Raindrop size distribution expressions. *J. Appl. Meteor.*, **15**, 1029–1031.

Marshall, J. S., and W. M. K. Palmer, 1948: The distribution of raindrops with size. *J. Meteor.*, **5**, 165–166.

Marzoug, M., and P. Amayenc, 1994: A class of single and dual frequency algorithms for rain-rate profiling from a spaceborne radar. *J. Atmos. Oceanic Technol.*, **11**, 1480–1506.

Schönhuber, M., H. E. Urban, W. L. Randeu, J. P. V. Poiares Baptista, and W. Riedler, 1996: Hydrometeor shapes and size distributions measured under various climatic conditions. *PIERS (Progress in Electromagnetics Research Symp.) '96*, Innsbruck, Austria, University of Innsbruck, 182 pp.

Sekhon, R. S., and R. C. Srivastava, 1971: Doppler radar observations of dropsize distributions. *J. Atmos. Sci.*, **28**, 983–994.

Sempere Torres, D., J. M. Porrà, and J.-D. Creutin, 1998: A general formulation for raindrop size distribution. *J. Geophys. Res.*, **103**, 1785–1797.

Srivastava, R. C., 1971: Size distribution of raindrops generated by their breakup and coalescence. *J. Atmos. Sci.*, **28**, 410–415.

——, 1988: On the scaling of equations governing the evolution of raindrop size distributions. *J. Atmos. Sci.*, **45**, 1091–1092.

Testud, J., E. Le Bouar, E. Obligis, and M. Ali Mehenni, 2000: The rain profiling algorithm applied to polarimetric weather radar. *J. Atmos. Oceanic Technol.*, **17**, 332–356.

Tokay, A., and D. A. Short, 1996: Evidence from tropical raindrop spectra of the origin of rain from stratiform versus convective clouds. *J. Appl. Meteor.*, **35**, 355–371.

Uijlenhoet, R., 1999: Parameterization of the rainfall microstructure for radar meteorology and hydrology. Thesis presented at Wageningen Agricultural University, 272 pp.

Ulbrich, C. W., 1983: Natural variations in the analytical form of the drop size distribution. *J. Climate Appl. Meteor.*, **22**, 1764–1775.

Urban, H. E., M. Schönhuber, W. L. Randeu, J. P. V. Poiares Baptista, and W. Riedler, 1996: Functional design aspects of a new 2D-video-distrometer. *PIERS (Progress in Electromagnetics Research Symp.) '96*, Innsbruck, Austria, University of Innsbruck, 271 pp.

Valdez, M. P., and K. Young, 1985: Number fluxes in equilibrium raindrop populations: A Markov chain analysis. *J. Atmos. Sci.*, **42**, 1024–1036.

Webster, P., and R. Lukas, 1992: TOGA COARE. The Coupled Ocean–Atmosphere Response Experiment. *Bull. Amer. Meteor. Soc.*, **73**, 1377–1416.

Williams, C. R., A. Kruger, K. S. Gage, A. Tokay, R. Cifelli, W. F. Krajewski, and C. Kummerow, 2000: Comparison of simultaneous rain drop size distributions estimated from two surface disdrometers and a UHF profiler. *Geophys. Res. Lett.*, **27**, 1763–1766.

Willis, P. T., 1984: Functional fits to some observed dropsize distributions and parameterization of rain. *J. Atmos. Sci.*, **41**, 1648–1661.

Zawadzki, I., and M. de Agostinho Antonio, 1988: Equilibrium raindrop size distribution in tropical rain. *J. Atmos. Sci.*, **45**, 3452–3459.

——, E. Monteiro, and F. Fabry, 1994: The development of drop size distribution in light rain. *J. Atmos. Sci.*, **51**, 1100–1113.